CEP78 functions downstream of CEP350 to control biogenesis of primary cilia by negatively regulating CP110 levels

André Brás Gonçalves[1,6], Sarah Kirstine Hasselbalch[1,7], Beinta Biskopstø Joensen[1,7], Sebastian Patzke[2], Pernille Martens[1], Signe Krogh Ohlsen[3], Mathieu Quinodoz[4,4.1,4.2], Konstantinos Nikopoulos[5], Reem Suleiman[1], Magnus Per Damsø Jeppesen[1], Catja Weiss[1], Søren Tvorup Christensen[1], Carlo Rivolta[4,4.1,4.2], Jens S. Andersen[3], Pietro Farinelli[1*] and Lotte Bang Pedersen[1*]

[1]Department of Biology, Section for Cell Biology and Physiology, University of Copenhagen, Universitetsparken 13, DK-2100 Copenhagen Ø, Denmark

[2]Department of Radiation Biology, Institute for Cancer Research, Norwegian Radium Hospital, Oslo University Hospital, Oslo, Norway

[3]Department of Biochemistry and Molecular Biology, University of Southern Denmark, Campusvej 55, 5230 Odense M, Denmark

[4]Institute of Molecular and Clinical Ophthalmology Basel (IOB), Basel, Switzerland

[4.1]Department of Ophthalmology, University of Basel, Basel, Switzerland

[4.2]Department of Genetics and Genome Biology, University of Leicester, Leicester, United Kingdom

[5]Department of Computational Biology, University of Lausanne, Switzerland

[6] Current address: Instituto de Medicina Molecular João Lobo Antunes, Faculdade de Medicina, Universidade de Lisboa, Lisbon, Portugal

[7]These authors contributed equally to this study

32 *For correspondance: Pietro.Farinelli@twelve.bio (PF); lbpedersen@bio.ku.dk (LBP)

Abstract

CEP78 is a centrosomal protein implicated in ciliogenesis and ciliary length control, and mutations in the *CEP78* gene cause retinal cone-rod dystrophy associated with hearing loss. However, the mechanism by which CEP78 affects cilia formation is unknown. Based on a recently discovered disease-causing *CEP78* p.L150S mutation, we identified the disease-relevant interactome of CEP78. We confirmed that CEP78 interacts with the EDD1-DYRK2-DDB1^{VPRBP} E3 ubiquitin ligase complex, which is involved in CP110 ubiquitination and degradation, and identified a novel interaction between CEP78 and CEP350 that is weakened by the CEP78^{L150S} mutation. We show that CEP350 promotes centrosomal recruitment and stability of CEP78, which in turn leads to centrosomal recruitment of EDD1. Consistently, cells lacking CEP78 display significantly increased cellular and centrosomal levels of CP110, and depletion of CP110 in CEP78-deficient cells restored ciliation frequency to normal. We propose that CEP78 functions downstream of CEP350 to promote ciliogenesis by negatively regulating CP110 levels via an EDD1-dependent mechanism.

Introduction

Primary cilia are antenna-like sensory organelles that play pivotal roles in coordinating various signaling pathways important for human development and tissue homeostasis [1]. They comprise a microtubule-based axoneme core, which extends directly from the mother centriole-derived basal body and is surrounded by a bilayer membrane enriched for specific receptors, ion channels and lipids that endow the organelle with unique signaling properties [2]. Not surprisingly, mutations in genes that affect assembly, structure or function of cilia are causative for a growing number of pleiotropic diseases and syndromes called ciliopathies, which include cone-rod dystrophy in the retina and hearing loss (CRDHL; MIM# 617236) amongst others [3]. Ciliopathy genes include those coding for components of the centrosome, which contains the daughter and mother centriole and gives rise to the ciliary basal body. The mother centriole is distinguished from the daughter centriole by distal and subdistal appendages, which play critical roles in vesicle docking at the onset of ciliogenesis and in microtubule anchoring, respectively. In addition, the centrosome contains pericentriolar material and is associated with centriolar satellites that affect cilia biogenesis and function in various ways [4].

Assembly of primary cilia is a complex, multistep process that is tightly coordinated with the cell cycle. In actively-proliferating cells, centriolar coiled coil protein 110 (CP110; also known as CCP110) and centrosomal protein of 97 kDa (CEP97) cap the distal ends of both mother and daughter centrioles and suppress ciliogenesis. Furthermore, overexpression of CP110 in growth-arrested cells prevents ciliogenesis [5]. CP110 also regulates centriole duplication and length control during S phase and interacts with key regulators of centriole duplication, including PLK4 [6-9]. As cells enter G1/G0, ciliogenesis begins with recruitment of pre-ciliary vesicles to the distal end of the mother centriole. The vesicles subsequently fuse to form a larger ciliary vesicle underneath which the ciliary transition zone and axoneme are assembled. The axoneme is further extended by intraflagellar transport (IFT), and the ciliary vesicle expands and matures to form the ciliary membrane and a surrounding sheath that fuses with the plasma membrane upon completion of ciliogenesis [10-12].

Initiation of transition zone formation and axoneme extension during early stages of ciliogenesis require removal of the CEP97-CP110 complex from the distal end of the mother centriole [5]. This process relies on M-Phase Phosphoprotein 9 (MPP9), which interacts directly with CEP97 and cooperates with kinesin KIF24 to recruit the CEP97-CP110 complex to the distal centriole end [13, 14]. During ciliogenesis, phosphorylation of MPP9 by Tau tubulin kinase 2 (TTBK2) leads to degradation of MPP9 by the ubiquitin proteasome system (UPS), which results in destabilization of

80 the CEP97-CP110 complex causing its removal from the distal end of the mother centriole [14].
81 TTBK2 is recruited to the mother centriole distal appendages by CEP164 [15, 16] where it also
82 phosphorylates CEP83 to promote CP110 removal [17]. Consequently, depletion of CEP164,
83 TTBK2, CEP83 or other centriole distal appendage proteins that regulate their localization and/or
84 function impairs ciliogenesis [18-23]. Mother centriole recruitment of TTBK2 and removal of the
85 distal CEP97-CP110 cap additionally requires the subdistal CEP350-FOP-CEP19 complex, which
86 furthermore interacts with RABL2 and IFT-B complex components to promote their axonemal en-
87 try [24-26].
88 Despite recent advances, the precise mechanisms by which CP110 regulates ciliogenesis and
89 is removed from the mother centriole at the onset of ciliogenesis remain incompletely understood.
90 For example, a recent study implicated the homologous to the E6AP carboxyl terminus (HECT)
91 type EDD1-DYRK2-DDB1^{VPRBP} E3 ligase complex in ubiquitination and degradation of CP110 via
92 a mechanism involving direct interaction of viral protein R binding protein (VPRBP; also known as
93 DCAF1) and centrosomal protein of 78 kDa (CEP78) [27]. Specifically, the authors reported that
94 CEP78 suppresses CP110 ubiquitination by EDD1 (also known as UBR5 and EDD) and it was pro-
95 posed that CP110 is phosphorylated by DYRK2 and thereby recognized and brought close to EDD1
96 by VPRBP. EDD1 then transfers ubiquitin to CP110 leading to its degradation. When CEP78 binds
97 VPRBP it induces a conformational change in the complex thereby preventing CP110 ubiquitina-
98 tion. Further, they demonstrated that depletion of CEP78 promoted centriole elongation, whereas
99 *CEP78* over-expression inhibited primary cilia formation in hTERT-immortalized retinal pigment
100 epithelial (RPE1) cells [27]. On the other hand, knockout (KO) of *Dyrk2* in the mouse was reported
101 to result in elongation of primary cilia, but centrosomal CP110 levels appeared unaffected in *Dyrk2*
102 mouse KO cells [28]. Therefore, it remains uncertain how CEP78 and the EDD1-DYRK2-
103 DDB1^{VPRBP} complex affect CP110 homeostasis to control ciliogenesis.
104 *CEP78* is composed of 16 exons and encodes a protein comprising 722 amino acids that
105 possesses five consecutive leucine rich repeats (LRR) at the N-terminus, and a coiled-coil (CC) do-
106 main at the C-terminus [29, 30]. Four independent studies have reported eight different mutations in
107 *CEP78* in patients with CRDHL [29-32], whereas one study identified a homozygous *CEP78*-trun-
108 cating variant in a family with non-syndromic retinitis pigmentosa (MIM# 268003; [33]), another
109 form of retinal degeneration. Of these studies, two have investigated the functional consequences of
110 human *CEP78* mutations at the cellular level. In one study, whole-exome sequencing (WES) identi-
111 fied biallelic mutations in *CEP78* in two unrelated families from Greece and Sweden, respectively

112 [29]. The Greek subject had a homozygous base substitution at the splice donor site in intron 3 of
113 *CEP78* (NM_032171.2:c.499+1G>T). Two subjects from a Swedish family carried heterozygous
114 mutations, one base substitution in intron 3 (NM_032171.2:c.499+5G>A) and a single nucleotide
115 deletion in exon 5 (NM_032171.2:c.633del; p.Trp212GlyfsTer18) causing a frameshift. These
116 *CEP78* mutations lead to exon skipping and premature stop codons accompanied by almost unde-
117 tectable levels of CEP78 protein in human skin fibroblasts (HSFs) of affected individuals. Further-
118 more, it was found that HSFs from these patients have significantly longer primary cilia as com-
119 pared to control cells [29]. More recently, a missense mutation in *CEP78*
120 (NM_032171.2:c.449T>C; p.Leu150Ser) was identified in three unrelated families from Belgium
121 and Germany diagnosed with CRDHL [30]. In the two Belgian families, affected individuals were
122 homozygous for the p.Leu150Ser variant, whereas affected individuals from the German family dis-
123 played compound heterozygosity for this variant and a novel splice site variant,
124 NM_032171.2:c.1462-1G>T. In all cases, HSFs from patients harboring the p.Leu150Ser mutation
125 (hereafter: L150S) displayed decreased cellular levels of CEP78 and significantly elongated cilia
126 compared to control HSFs [30], as seen in patient-derived HSFs with CEP78 truncating mutations
127 [29]. In addition, other ciliopathy features were reported in some of the affected individuals with the
128 $CEP78^{L150S}$ mutation, including obesity, respiratory problems, diabetes 2 and infertility [30]. In
129 summary, available data derived from human patients indicates that depletion of CEP78 leads to
130 elongation of primary cilia at the cellular level, which manifests in ciliopathy phenotypes at the or-
131 ganism level. However, the mechanism by which CEP78 regulates ciliary length is not known.
132 In addition to the patient studies described above, some studies have addressed CEP78 func-
133 tion in different cell culture models. First, a study showed that siRNA-mediated depletion of CEP78
134 in RPE1 cells reduces the frequency of cells forming primary cilia, possibly due to centriolar an-
135 choring defects, but the length of the residual cilia was not assessed. Similarly, depletion of CEP78
136 in *Planarians* was shown to impair motile cilia formation due to defective docking of centrioles to
137 the cell surface [34]. Another study identified CEP78 interaction with PLK4 and implicated CEP78
138 in PLK4-mediated centriole over duplication, whereas possible roles for CEP78 in relation to cilia
139 were not addressed [35]. Finally, as mentioned above, a study reported that CEP78 directly interacts
140 with VPRBP of the EDD1-DYRK2-$DDB1^{VPRBP}$ E3 ligase complex to suppress CP110 ubiquitina-
141 tion and thereby stabilize it [27]. How such CEP78-mediated stabilization of CP110 might lead to
142 the long cilia phenotype observed in patient fibroblasts lacking CEP78 [29, 30] and/or the reduced
143 ciliation frequencies seen in CEP78-depleted *Planarians* and RPE1 cells [34] is unclear.

144 Here were show that in RPE1 cells and patient-derived HSFs loss of CEP78 leads to reduced
145 ciliation frequency as well as increased length of the cilia that do form. Further, we find that a mu-
146 tant line expressing a partially functional, truncated version of CEP78 displays reduced ciliation fre-
147 quency but normal length of residual cilia. By taking advantage of the recently identified disease-
148 causing $CEP78^{L150S}$ mutation [30], we used a quantitative mass spectrometry-based approach to
149 identify a disease-relevant interactome of CEP78. We confirmed that CEP78 interacts with the
150 EDD1-DYRK2-$DDB1^{VPRBP}$ complex implicated in CP110 ubiquitination and degradation [27], and
151 furthermore identified a novel interaction between CEP78 and the N-terminal region of CEP350.
152 The interaction of CEP78 with both VPRBP and CEP350, as well as centrosomal recruitment of
153 CEP78, are dramatically reduced by the $CEP78^{L150S}$ mutation. Lack of centrosomal recruitment of
154 $CEP78^{L150S}$ is likely due to impaired interaction with CEP350 since centrosomal and cellular levels
155 of CEP78 were significantly decreased in *CEP350* KO cells. Conversely, cells lacking CEP78 dis-
156 played significantly decreased centrosomal levels of EDD1 and unaltered or slightly increased cen-
157 trosomal levels of VPRBP and CEP350. In addition, CEP78-deficient cells showed significantly in-
158 creased cellular and centrosomal levels of CP110, presumably owing to the reduced centrosomal
159 levels of EDD1 observed in these cells. Depletion of CP110 in CEP78-deficient cells restored cilia-
160 tion frequency, but not the increased length of remaining cilia, to normal. Collectively our results
161 suggest that CEP78 functions downstream of CEP350 to promote cilia biogenesis by negatively
162 regulating CP110 levels via an EDD1-dependent mechanism, but suppresses ciliary elongation in-
163 dependently of CP110.
164

165 ## Results

166 **Depletion of CEP78 leads to fewer and longer primary cilia in cultured cells**

167 Previous studies showed that patient-derived fibroblasts lacking CEP78 display significantly elon-
168 gated primary cilia compared to control cells [29, 30] whereas depletion of CEP78 in *Planarians*
169 and RPE1 cells was shown to significantly reduce cilia numbers [34]. To reconcile these seemingly
170 contradictory findings we analyzed cilia numbers and length in serum-deprived wild type (WT)
171 RPE1 cells and four different *CEP78* KO clones generated by CRISPR/Cas9 methodology. We first
172 confirmed by western blot analysis with CEP78-specific antibody that endogenous CEP78 is lack-
173 ing in three of the mutant clones, designated #2, #52 and #73, whereas clone #44 expresses a
174 shorter version of CEP78 (Figure 1-figure supplement 1A). Sequencing of clone #44 indicated that
175 it contains an insertion of the px459-Cas9 plasmid in exon 1 of *CEP78*, suggestion that a shorter

176 version of CEP78 lacking the extreme N-terminus is expressed in this strain, possibly from an alter-
177 native promoter. Immunofluorescence microscopy (IFM) analysis with antibodies against ciliary
178 (ARL13B) and centrosomal (CEP350) markers showed that the frequency of ciliated cells is signifi-
179 cantly reduced in all four *CEP78* KO clones compared to WT cells (Figure 1A, B; Figure 1-Figure
180 supplement 1B). In addition, the length of the remaining cilia was significantly increased in the
181 three *CEP78* KO clones that completely lack CEP78, but identical to the average WT cilia size in
182 clone #44 (Figure 1A, C; Figure 1-figure supplement 1C). The latter result indicates that the trun-
183 cated CEP78 protein expressed in clone #44 functions normally with respect to ciliary length con-
184 trol, in turn suggesting that CEP78 may affect ciliogenesis and ciliary length by distinct mecha-
185 nisms. For the rest of this manuscript RPE1 *CEP78* KO cells refer to clone #73 unless otherwise
186 indicated.
187 In agreement with our observations in RPE1 cells, similar results were obtained using previ-
188 ously described patient-derived *CEP78*-deficient or control HSFs (Figure 1D-F) [29, 30]. The low
189 ciliation frequencies of serum-deprived *CEP78* mutant cells were not secondary to cell cycle de-
190 fects, as judged by western blot analysis with antibody against retinoblastoma protein phosphory-
191 lated at S807/811 (P-Rb; Figure 1G-L). However, in serum-fed cells, P-Rb levels were significantly
192 higher in *CEP78* mutant cells compared to controls (Figure 1G-L), indicating that mutant cells may
193 progress slower through S-phase [36]. This is in line with previous reports indicating that CEP78
194 protein levels are upregulated in late S-G2 phase suggesting a role for CEP78 at this cell cycle
195 stage, e.g. during centriole duplication [27, 35]. We conclude that CEP78 deficient RPE1 and HSF
196 cells display reduced ciliation frequencies as well as increased length of remaining cilia, thus recon-
197 ciling previous observations [29, 30, 34].
198
199 **Analysis of RPE1 WT and *CEP78* KO cells expressing FLAG- or mNG-tagged CEP78 or**
200 **CEP78^{L150S} fusions**
201 To confirm the above results, we first set out to perform a rescue experiment by expressing FLAG-
202 CEP78 in WT and *CEP78* KO RPE1 cells followed by serum-deprivation and IFM analysis using
203 FLAG and ARL13B antibodies. In parallel, we performed similar experiments with FLAG-
204 CEP78^{L150S}. We first analyzed the localization and expression levels of the two FLAG fusions in
205 transiently transfected serum-deprived RPE1 cells. In 4% paraformaldehyde-fixed cells we ob-
206 served that the ARL13B antibody labeled the cilium itself as well as the basal body, but not the
207 daughter centriole. The basal body pool of ARL13B likely corresponds to that present in the mother

208 centriole-associated vesicle of mitotic centrosomes [37]. The transiently expressed FLAG-CEP78
209 fusion protein localized to both centrioles at the base of cilia as expected [27, 29, 35], whereas cen-
210 triolar localization of FLAG-CEP78^{L150S} was severely compromised although not completely abol-
211 ished (Figure 2A, B). The latter result is in line with previous reports showing that the LRR region
212 in the N-terminus of CEP78, which encompasses residue L150, is important for its localization to
213 centrioles [27, 35]. Both FLAG fusions were expressed at similar levels in the cells (Figure 2-figure
214 supplement 1); this was somewhat surprising given that endogenous CEP78^{L150S} is largely undetect-
215 able by western blot analysis of patient-derived HSFs suggesting its stability is compromised [30].
216 Therefore, we tested if the L150S mutation might affect binding of the CEP78 antibody used in [30]
217 to CEP78. However, FLAG immunoprecipitation (IP) and western blot analysis of 293T cells ex-
218 pressing FLAG-CEP78 or FLAG-CEP78^{L150S} indicated that the CEP78 antibody binds equally well
219 to WT CEP78 and the CEP78^{L150S} mutant protein. This analysis also revealed that endogenous
220 CEP78 co-IPs with FLAG-CEP78 indicating that CEP78 can form homodimers/oligomers (Figure
221 2-figure supplement 2). These results indicate that the L150S mutation compromises the recruit-
222 ment of CEP78 to the centrosome, but not its short-term stability, at least in RPE1 cells. We cannot
223 rule out that the N-terminal FLAG tag may stabilize FLAG-CEP78^{L150S} and prevent it from being
224 degraded.
225 Next, we tested if FLAG-CEP78 or FLAG-CEP78^{L150S} could rescue the ciliary phenotypes
226 of *CEP78* KO cells. However, upon transient expression of the FLAG-CEP78 fusions we could not
227 rescue the cilia frequency and length phenotype of the *CEP78* KO cells, and cilia frequency and
228 length were also affected in WT control cells transiently expressing these fusions (data not shown).
229 We therefore generated cell lines stably expressing mNeonGreen (mNG)-tagged CEP78 or
230 CEP78^{L150S} at ca. 3-4 times the endogenous CEP78 level by viral transduction of mNG-CEP78 con-
231 structs into WT and *CEP78* KO RPE1 cells, respectively (Figure 2-figure supplement 3A). Micro-
232 scopic examination of these lines indicated that mNG-CEP78 was concentrated at the centrosome as
233 expected, whereas mNG-CEP78^{L150S} was diffusely located in the cytosol (Figure 2-figure supple-
234 ment 3B), in agreement with results for transiently expressed FLAG-CEP78/CEP78^{L150S} fusions
235 (Figure 2A, B). Importantly, stably expressed mNG-CEP78 could fully rescue the ciliation fre-
236 quency phenotype of *CEP78* KO cells whereas mNG-CEP78^{L150S} could not (Figure 2C). In addi-
237 tion, we observed that WT cells stably expressing mNG-CEP78 have significantly reduced ciliation
238 frequency compared to untransfected WT cells (Figure 2C), indicating that mild overexpression of
239 mNG-CEP78 seems to inhibit ciliogenesis. Furthermore, WT or *CEP78* KO cells stably expressing

240 mNG-CEP78 had significantly shorter cilia than untransfected WT and *CEP78* KO cells, or *CEP78*
241 KO cells expressing mNG-CEP78^{L150S}. However, we note that cilia length in the latter was signifi-
242 cantly shorter than untransfected *CEP78* KO cells (Figure 2D). Together these results suggest that
243 mNG-CEP78 is able to fully rescue the cilia frequency phenotype of *CEP78* KO cells whereas
244 mNG-CEP78^{L150S} is not. Furthermore, both mNG-CEP78 and mNG-CEP78^{L150S} promote ciliary
245 shortening, but mNG-CEP78 does it more efficiently than mNG-CEP78^{L150S}. We conclude that the
246 observed ciliary frequency and length phenotypes of the *CEP78* KO cells are caused specifically by
247 CEP78 loss, and that the L150S mutations impairs CEP78 centrosome localization and function.
248

249 **CEP78 interacts with the EDD1-DYRK2-DDB1^{VPRBP} complex and CEP350**

250 To explore how CEP78 is recruited to centrioles to regulate ciliary frequency and length we first
251 used Stable Isotope Labeling by Amino acids in Cell culture (SILAC)-based quantitative mass spec-
252 trometry (MS) to identify the differential interactomes of FLAG-CEP78 and FLAG-CEP78^{L150S} ex-
253 pressed in 293T cells (see Materials and methods for details). We identified interaction between
254 CEP78 and several components of the EDD1-DYRK2-DDB1^{VPRBP} complex (Figure 3A), in agree-
255 ment with previous work showing direct binding of CEP78 to VPRBP within this complex [27]. In-
256 terestingly, the MS results indicated that the CEP78^{L150S} mutation dramatically reduces this interac-
257 tion (Figure 3A), which we confirmed by IP and western blot analysis of 293T cells co-expressing
258 Myc-VPRBP and FLAG-CEP78 or FLAG-CEP78^{L150S} (Figure 3B). In addition, our interactome
259 analysis identified CEP350 as potential novel CEP78 binding partner (Figure 3A). Using IP and
260 western blot analysis in 293T cells co-expressing FLAG-CEP78 or FLAG-CEP78^{L150S} with a Myc-
261 tagged N-terminal or C-terminal CEP350 truncation we found that CEP78 binds to the N-terminal
262 region of CEP350 (residues 1-983; Figure 3C, E); reciprocal co-IP with Myc-tagged CEP350 con-
263 structs confirmed this result (Figure 3-figure supplement 1A). Furthermore, we found that the inter-
264 action between CEP78 and CEP350 N-terminus is reduced by the CEP78^{L150S} mutation (Figure 3C).
265 Using a similar approach, we could not detect interaction between CEP78 and endogenous FOP
266 (Figure 3C), whereas under similar conditions endogenous FOP was readily co-IPed with the C-ter-
267 minus of CEP350 (Figure 3-figure supplement 1A), in agreement with a previous report [38]. We
268 also mapped the CEP350 interaction site in CEP78 and found that CEP350 primarily binds to the C-
269 terminal region of CEP78 comprising residues 395-722 (Figure 3D, E), although a weak interaction
270 with a fragment comprising the entire LRR region (residues 2-403) was also observed. In contrast,
271 truncation of the latter fragment into two smaller fragments abolished binding to the CEP350 N-

272 terminus (Figure 3D, E). Binding of CEP78 to VPRBP similarly requires the entire LRR region of
273 CEP78 [27] and we therefore wondered whether interaction between CEP350 and CEP78 might be
274 mediated by VPRBP. However, Myc IP experiments and western blot analysis failed to reveal
275 physical interaction between VPRBP and Myc-CEP350 N-terminus (Figure 3, figure supplement
276 1A). Moreover, GFP IP of cells co-expressing GFP-CEP78 and Myc-CEP350 N- or C-terminal
277 fragments showed that GFP-CEP78 can bind to Myc-CEP350 N-terminus and endogenous VPRBP
278 at the same time, indicating that CEP350 does not compete with VPRBP for binding to CEP78
279 (Figure 3, figure supplement 1B). We conclude that CEP78 binds independently to VPRBP and the
280 N-terminus of CEP350 and that both of these interactions are reduced by the CEP78^{L150S} mutation.
281
282 **CEP350 regulates the stability and centrosomal recruitment of CEP78**
283 In non-ciliated HeLa and U2OS cells endogenous CEP78 was reported to localize to both centrioles
284 during all phases of the cell cycle and appeared to concentrate at the centriole wall [35]. In ciliated
285 RPE1 cells CEP78 was shown to localize to the distal end of both centrioles, with a preference for
286 the mother centriole/basal body [27]. Similarly, CEP350 was reported to localize to the distal end of
287 the mother centriole/basal body, near the subdistal appendages, in ciliated RPE1 cells [24, 26, 39].
288 In agreement with these reports and with our interactome and IP results (Figure 3), 3D Structured
289 Illumination Microscopy (SIM) showed partial co-localization of mNG-CEP78 with CEP350 at the
290 distal end of the centrioles in RPE1 cells, adjacent to the distal appendage marker CEP164 and the
291 centriole capping complex protein CP110 (Figure 4A). Superimposing fluorescence images on elec-
292 tron micrographs of the mother centriole [40] indicates that mNG-CEP78 localizes to a ring-struc-
293 ture of centriole-sized diameter at the distal half of the centriole, encompassed by a wider unclosed
294 ring-structure of CEP350. mNG-CEP78 but not CEP350 depicted decreased levels at the daughter
295 centriole as compared to the mother. Furthermore, using a previously characterized RPE1 *CEP350*
296 KO cell line [24] that displays significantly reduced centrosomal levels of CEP350 (Figure 4-figure
297 supplement 1), we found that depletion of CEP350 not only reduces localization of CEP78 to the
298 centrosome, but also its total cellular level (Figure 4B-G). Similarly, we found significantly reduced
299 levels of CEP78 in *FOP* KO cells (Figure 4 B, C), in line with the decreased centrosomal levels of
300 CEP350 observed in these cells [24]. These results indicate that CEP350 promotes the recruitment
301 of CEP78 to the mother centriole/basal body as well as its overall stability.
302
303 **CEP78 mutant cells display reduced centrosomal levels of EDD1**

304 Next, we asked if CEP78 might affect the centrosomal recruitment of components of the EDD1-
305 DYRK2-DDB1^{VPRBP} complex and/or CEP350, and analyzed the cellular or centrosomal levels of
306 relevant complex components in RPE1 WT and *CEP78* KO cells. The results showed that serum-
307 deprived, ciliated *CEP78* KO cells display significantly increased centrosomal levels of CEP350
308 (Figure 5A, B) as compared to controls. However, in serum-deprived, non -ciliated cells, the centro-
309 somal levels of CEP350 were not significantly different in *CEP78* KO cells compared to WT con-
310 trols (Figure 5C, D). Similar results were obtained for CEP350 in control and CEP78 deficient pa-
311 tient HSFs (Figure 5E-H). We also analyzed the cellular levels of VPRBP by western blotting and
312 the centrosomal levels of VPRBP and EDD1 by IFM in RPE1 WT and *CEP78* KO cells. In agree-
313 ment with a previous study [27] we found that cellular and centrosomal levels of VPRBP were not
314 significantly reduced in serum-fed or serum-deprived *CEP78* KO cells compared to controls (Fig-
315 ure 6A-C; Figure 6-figure supplement 1). Thus, CEP78 seems to be dispensable for recruitment of
316 VPRBP and CEP350 to the centrosome. In contrast, centrosomal levels of EDD1 were significantly
317 reduced in RPE1 *CEP78* KO cells compared to WT controls, both in ciliated and non-ciliated cells
318 (Figure 6D-G). Thus, CEP78 is required for efficient recruitment of EDD1 to the centrosome. To
319 corroborate this result, we measured the centrosomal levels of EDD1 in RPE1 *CEP350* KO cells
320 and found that EDD1 levels were also significantly reduced when compared to the controls (Figure
321 6-figure supplement 2). Together our data indicate that CEP350, by recruiting CEP78 to the centro-
322 some, also promotes the centrosomal recruitment of EDD1.
323
324 **Increased cellular and centrosomal levels of CP110 in CEP78 deficient cells**
325 Since EDD1 is an E3 ubiquitin-protein ligase that negatively regulates CP110 levels [27], and
326 whose depletion impairs ciliogenesis [41, 42], we asked if the loss of CEP78 would lead to altered
327 levels of CP110 at the centrosome. Indeed, western blot and IFM analysis of RPE1 WT and *CEP78*
328 KO cells revealed that total cellular and centrosomal CP110 levels are significantly increased in
329 *CEP78* KO cells compared to WT controls, both under serum-deprived (Figure 7A-D, F, G; Figure
330 7-figure supplement 1A, B) and serum-fed conditions (Figure 7-figure supplement 2A-D), whereas
331 CP110 levels appeared normal upon stable expression of mNG-CEP78 in the *CEP78* KO back-
332 ground (Figure 7-figure supplement 1C). We also analyzed CP110 levels specifically at the mother
333 centriole of ciliated RPE1 WT and *CEP78* KO cells and found no significant differences between
334 them (Figure 7E). Similar results were obtained using *CEP78* mutant and control HSF cells (Figure
335 7G-H). Since a previous study reported that siRNA-mediated depletion of CEP78 in RPE1 and

336 HeLa cells reduces the cellular levels of CP110 [27], a result contradicting our own observations
337 (Figure 7; Figure 7-figure supplement 1 and 2), we tested if the elevated CP110 levels seen in our
338 *CEP78* mutant cells might be due to compensatory upregulation of CP110 mRNA expression.
339 However, RNA-Seq analysis indicated no significant changes in CP110 mRNA levels in patient-
340 derived, *CEP78* deficient HSF cultures compared to controls; mRNA levels of CEP350, VPRBP
341 and DDB1 in *CEP78* deficient HSF cultures were also similar to those of controls (Figure 7-figure
342 supplement 3). Furthermore, a cycloheximide chase experiment indicated that CP110 is more stable
343 upon serum deprivation of *CEP78* KO cells compared to WT controls (Figure 7-figure supplement
344 4). Taken together, we conclude that loss of CEP78 leads to elevated cellular and centrosomal lev-
345 els of CP110 and that this is likely due to increased stability of CP110. Furthermore, our results in-
346 dicate that in ciliated *CEP78* KO cells, the amount of CP110 present specifically at the mother cen-
347 triole is not significantly higher than in control cells.
348
349 **Partial depletion of CP110 normalizes ciliation frequency of *CEP78* KO cells**
350 CP110 is a key negative regulator of ciliogenesis [5, 43] that was also shown to be required for cili-
351 ogenesis initiation as well as ciliary length control [44, 45]. The above results therefore prompted us
352 to test if the reduced ciliation frequency and/or increased length of remaining cilia observed in
353 *CEP78* deficient cells could result from elevated centrosomal CP110 levels in these cells. When we
354 used siRNA to partially deplete cellular and centrosomal CP110 from RPE1 WT and *CEP78* KO
355 cells and subjected the cells to serum deprivation (Figure 8A, B; Figure 8-figure supplement 1), we
356 found that the *CEP78* KO cells restored their ciliation frequency to WT levels, whereas partial
357 CP110 depletion had little effect on cilia numbers in WT cells grown under similar conditions (Fig-
358 ure 8C, D). In contrast, depletion of CP110 from *CEP78* KO cells did not rescue the ciliary length
359 defect of residual cilia; these cilia were still significantly longer than those of WT controls (Figure
360 8C, E). Thus, partial depletion of CP110 from *CEP78* KO cells can rescue their reduced ciliation
361 frequency phenotype but not the increased length of remaining cilia. This result is in line with our
362 observation that a *CEP78* KO clone expressing a truncated version of CEP78 (clone #44) displays
363 significantly reduced ciliation frequency, but normal length of the cilia that do form (Figure 1-fig-
364 ure supplement 1), implying that CEP78 regulates ciliogenesis and ciliary length by separate mech-
365 anisms.
366
367 **Discussion**

368 Several studies have shown that loss-of-function mutations in *CEP78* are causative of ciliopathy
369 characterized by CRDHL [29-32], and that cells lacking CEP78 display reduced ciliation frequency
370 [34] or abnormally long cilia [29, 30]. However, the molecular mechanisms by which CEP78 regu-
371 lates cilium biogenesis and length were so far unclear. In this study, we found that loss of CEP78
372 leads to decreased ciliation frequency as well as increased length of the residual cilia that do form,
373 both in RPE1 cells and patient-derived HSFs. Recue experiments in *CEP78* KO RPE1 cells stably
374 expressing mNG-CEP78 or mNG-CEP78^{L150} supported that the observed phenotypes were specifi-
375 cally caused by loss of CEP78 at the centrosomes. Interestingly, we found that both ciliated and
376 non-ciliated CEP78 deficient cells fail to efficiently recruit EDD1 to the centrosome, whereas cellu-
377 lar and overall centrosomal levels of CP110 are dramatically increased. However, in the subpopula-
378 tion of *CEP78* KO cells that are ciliated, CP110 levels specifically at the mother centriole were sim-
379 ilar to those of ciliated control cells, implying that the elevated centrosomal CP110 level observed
380 in these cells is caused by a pool of CP110 located at the daughter centriole and/or pericentriolar
381 area. This result also indicates that the abnormally long cilia phenotype seen in the *CEP78* KO cells
382 is not caused by increased CP110 levels at the mother centriole. Supportively, siRNA-mediated de-
383 pletion of CP110 could restore cilia frequency, but not length, to normal in the *CEP78* KO cells.
384 Furthermore, a *CEP78* mutant line, clone #44, expressing a shorter version of CEP78 likely lacking
385 the N-terminus displayed reduced ciliation frequency but normal length of residual cilia, substanti-
386 ating that CEP78 regulates ciliogenesis and cilia length by distinct mechanisms. Specifically, our
387 results indicate that CEP78 promotes ciliogenesis by negatively regulating CP110 levels at the
388 mother centriole via activation of VprBP, but negatively regulates ciliary lengthening independently
389 of CP110 (Figure 8F).
390 The removal of CP110 from the distal end of the mother centriole constitutes a key step in
391 the initiation of ciliogenesis and is regulated by a growing number of proteins that include TTBK2
392 [19] and components of the UPS system such as Neurl-4 [46] and the cullin-3 (CUL3)–RBX1–
393 KCTD10 complex [47]. The EDD1-DYRK2-DDB1^{VPRBP} complex was similarly shown to mediate
394 degradation of CP110 and to interact with CEP78 [27], but the precise consequences of these activi-
395 ties for ciliogenesis were unclear. Our work strongly suggests that CEP78 functions together with
396 the EDD1-DYRK2-DDB1^{VPRBP} complex to negatively regulate centrosomal CP110 levels at the on-
397 set of ciliogenesis, leading to its removal from the distal end of the mother centriole (Figure 8F).
398 This is in contrast to a previously proposed model, which suggested that CEP78 inhibits degrada-
399 tion of CP110 by the EDD1-DYRK2-DDB1^{VPRBP} complex [27]. The reason for this discrepancy is

400 unclear, but may be due to different experimental approaches used in our study and the paper by
401 Hossain et al. [27]. In this latter study, siRNA was used to partially deplete CEP78 from cultured
402 cells, whereas we performed our experiments on cells with endogenous *CEP78* mutations. CP110
403 removal from the distal end of the mother centriole occurs concomitantly with docking of the cen-
404 triole to vesicles or the plasma membrane at the onset of ciliogenesis [12]. Therefore, a role for
405 CEP78 in removal of CP110 from the centrosome is compatible with ultrastructural analyses in *Pla-*
406 *narians*, which indicated that basal bodies fail to dock to the plasma membrane in CEP78 RNAi-
407 depleted animals [34]. Although not addressed in detail in the current study, the elevated centro-
408 somal CP110 levels observed in serum-fed CEP78 deficient cells are also compatible with previous
409 work implicating CEP78 in regulation of PLK4-mediated centriole duplication [35].
410 We also uncovered a new physical interaction between CEP78 and the N-terminal region of
411 CEP350, and found that CEP350 is important for recruitment of CEP78 to the centrosome as well
412 as for its overall stability. The reduced interaction of the CEP78^{L150S} mutant protein with CEP350
413 might explain its lack of detection by western blot analysis of patient HSFs [30], since reduced in-
414 teraction with CEP350 is likely to decrease the long-term stability of CEP78^{L150S}. Our IP and IFM
415 results furthermore suggests that CEP350 controls CP110 removal from the mother centriole not
416 only via recruitment of TTBK2 [24], but also via CEP78-dependent recruitment of EDD1. Indeed,
417 we observed reduced centrosomal levels of EDD1 in *CEP350* KO cells, consistent with this idea. It
418 remains to be determined whether these two pathways act in sequence or in parallel to control cen-
419 trosomal CP110 levels. Furthermore, as the recruitment of CEP350 to centrioles itself depends on
420 FOP [24, 26, 38] and on the distal centriole protein C2CD3 [14], loss of these proteins may simi-
421 larly affect the centrosomal recruitment of CEP78 and EDD1, and thereby negatively regulate
422 CP110 levels via this pathway. It will be important to investigate these possibilities in future stud-
423 ies.
424 While increased CP110 levels can account for the decreased ciliation frequency observed in
425 serum-deprived CEP78 mutant cells, it remains unclear why some of these cells form abnormally
426 long cilia. Our analysis indicated that the ciliated mutant cells are able to locally displace or degrade
427 CP110 at the mother centriole, but the underlying mechanism remains to be determined. Of note,
428 the *CEP350* KO cells used in our study also seem to display a similar dual phenotype, since approx-
429 imately 30% of these cells form cilia despite an inability to recruit TTBK2 and remove CP110 from
430 the mother centriole [24]. Moreover, a recent genome-wide siRNA knockdown analysis showed
431 that depletion of DDB1 caused an elongated cilia phenotype whereas depletion of EDD1 (UBR5)

432 lead to fewer but normal length cilia [48], even though DDB1 and EDD1 are part of the same E3
433 ubiquitin ligase complex [49]. Thus, a slight imbalance in the regulation of this complex might de-
434 termine whether or not cilia are formed and how long they are. It should also be noted that some
435 studies have reported dual roles for CP110 during ciliogenesis, i.e. CP110 may not only function to
436 inhibit ciliogenesis but may also promote ciliary extension in some contexts [44, 45]. Although the
437 mechanism responsible for the elongated cilia phenotype seen in some of the CEP78 mutant cells
438 remains unclear, one attractive candidate to be involved is CEP350, which we found to be present at
439 abnormally high levels at the centrosome of ciliated *CEP78* KO cells, specifically. Consistent with
440 this idea, we have observed that the CEP78 truncation mutant (clone #44), which expresses fewer,
441 but normal length cilia, displays normal or slightly reduced levels of CEP350 at the centrosome in
442 ciliated as well as in non-ciliated cells (data not shown). Alternatively, one or more substrates of
443 EDD1 other than CP110 could also be affected in the *CEP78* mutant cells thereby affecting ciliary
444 length control. For example, EDD1 was also shown to mediate ubiquitination of CSPP-L in turn
445 promoting its recruitment to centriolar satellites and the centrosome [42]. CSPP-L is a well-known
446 positive regulator of primary cilia formation [50] that was recently shown to bind directly to
447 CEP104 to control axoneme extension [51]. Furthermore, CEP104 is implicated in ciliogenesis
448 through interaction with the CEP97-CP110 complex and modulation of microtubule dynamics at
449 the ciliary tip [51-53]. It will therefore be interesting to investigate if and how CSPP-L and CEP104
450 localization is affected in CEP78 mutant cells. Moreover, as CEP350 additionally binds to CYLD
451 [54], a deubiquitinase that controls centriolar satellite homeostasis and ciliogenesis through de-
452 ubiquitination of the E3 ubiquitin ligase MIB1 [55, 56], and was proposed to regulate axonemal IFT
453 particle injection through FOP-CEP19-RABL2 interactions [24-26], it is tempting to speculate that
454 CEP78 might impinge on these processes.
455

456 ## Materials and methods

457

458 **PCR and cloning**

459 For the establishment of the N-terminal FLAG-tagged CEP78 construct a cDNA clone coding for
460 human full-length CEP78 cDNA (GeneCopoiea pShuttle™Gateway® PLUS ORF, NCBI accession
461 number NM_001098802) was used as template for amplification with the Phusion High-Fidelity
462 DNA polymerase (New England BioLabs) under standard PCR conditions and attB forward and re-
463 verse primers (see Key Resources Table) compatible with the Gateway cloning technology

464 (Invitrogen/Thermo Fisher Scientific) for inclusion of the insert into the pDonor201 Gateway vector
465 (Invitrogen/Thermo Fisher Scientific). To produce human FLAG-CEP78^{L150S}, site directed muta-
466 genesis was performed with QuickChange Lightning Site-Directed Mutagenesis Kit (Agilent) and
467 primers CEP78 mut_F and CEP78 mut_R (see Key Resources Table). Accuracy of the *CEP78*
468 ORF was assessed by Sanger sequencing. Subsequently, the desired fragment was cloned into
469 p3xFLAG-CMV/DEST (gift from Dr. Ronald Roepman lab, Radboud University Medical School,
470 Nijmegen, NL; see Key Resources Table for details) to produce p3xFLAG-CEP78 or p3xFLAG-
471 CEP78^{L150S}.
472 Plasmids encoding full-length and truncated versions (N-terminus, middle, N-terminus plus
473 middle, C-terminus) of CEP78 tagged with GFP in the N-terminus were generated by PCR using
474 relevant primers (see Key Resources Table) and pFLAG-CEP78 as template; PCR products were
475 cloned into pEGFP-C1 by standard approaches, following digestion with BamHI (Roche, cat#
476 1056704001) and KpnI (Roche, cat#10899186001) and ligation with T4 DNA ligase (Applichem,
477 cat# A5188). Ligated plasmids were transformed into competent *E. coli* DH10B cells and cells har-
478 boring recombinant plasmids selected on Luria Bertani (LB; Sigma-Aldrich) agar plates with 50
479 μg/ml kanamycin. Plasmids were purified using Plasmid DNA Mini Kit I (Omega Biotech, cat#
480 D6943-02) or Nucleobond Xtra Mid kit (Macherey-Nagel, cat# 740410.50), according to protocols
481 supplied by the manufacturers. Sequences of plasmid inserts were verified by Eurofins Genomics.
482 Gateway system compatible pENTR vectors encoding for mNeonGreen-CEP78 or mNeon-
483 Green-CEP78L150S fusions were generated by subcloning of ORFs from pEGFP constructs de-
484 scribed above in frame with mNeonGreen using the BamH1/Kpn1 sites. For lentivirus particle pro-
485 duction these plasmids were recombined with pCDH-EF1a-Gateway-IRES-BLAST plasmids as de-
486 scribed in [51] using LR Clonase II (Invitrogen/Thermo Fisher Scientific).
487
488 **Mammalian cell culture and transfection**
489 Human skin fibroblasts were cultured as described previously [29, 30]. Human embryonic kidney-
490 derived 293T cells were cultured and transfected with plasmids as described previously [61]. RPE1
491 cells were grown in T-75 flasks in a 95% humidified incubator at 37 ºC with 5% CO2. Cells were
492 cultured in Dulbecco's Modified Eagle Medium (DMEM) (GIBCO®, cat# 41966-029) supple-
493 mented with 10% fetal bovine serum (FBS) and 1% penicillin/streptomycin (P/S). When cells were
494 about 80-90% confluent, they were passaged and set up for new experiments. Upon seeding, RPE1
495 cells were washed once with preheated 1 x phosphate buffered saline (PBS) and then incubated with

496 1% Trypsin-EDTA (ethylenediaminetetraacetic acid) (Sigma-Aldrich, cat# T4174) solution for 5
497 min at 37 ºC. The detached cells were aspired in an appropriate volume of new preheated DMEM
498 and seeded into petri dishes with or without sterile glass coverslips [62]. When the cells had reached
499 80-90% confluency they were serum starved for 24 hours to induce formation of primary cilia. A
500 small amount of cell solution was passaged on in a new T-75 flask containing new preheated
501 DMEM. All cell lines were tested negative for Mycoplasma and those not generated in this study
502 have been used in prior publications. New cell lines generated in this study were validated by
503 sanger sequencing.
504 For transfection with plasmids, RPE1 cells were seeded in 60 mm petri dishes as described
505 above to about 50-70% confluency at the time of transfection. For rescue experiments, 2 µg
506 pFLAG-CEP78 or pFLAG-CEP78^{L150S} and 6 µl FuGENE®6 were mixed in 100 µl serum- and anti-
507 biotic free DMEM and incubated for 20 minutes at room temperature. New DMEM was added to
508 the cells prior to transfer of the transfection reagent, which was gently dripped onto the cells and
509 swirled to make sure it was dispersed well. After cells were incubated with transfection medium
510 for 4 hours, the medium was replaced with serum free DMEM for 24 hours to induce growth arrest.
511 Gene silencing in RPE1 cells by siRNA was performed using DharmaFect (see Key Resources Ta-
512 ble). Briefly, RPE1 cells were seeded in DMEM medium with serum and antibiotics in 30 mm petri
513 dishes at 20-25% confluency. Transfection was performed by combining 50 nM siRNA with 5 µl of
514 DharmaFect in 200 µl of serum and antibiotic-free DMEM medium for 15 min at room tempera-
515 ture. After incubation, the complexes were added dropwise onto the cells and the media was swirled
516 gently to ensure good dispersion prior to incubation at 37 °C. Cells were kept under these condi-
517 tions for 48 hours and then serum starved for 24 hours before being processed for further experi-
518 ments.
519 RPE1 cell transduction with lentivirus particles and Blasticidine selection (10µg/ml f.c.) was
520 conducted as described in [51].
521
522 **Immunofluorescence microscopy and image analysis**
523 Standard epifluorescence IFM analysis was performed as described previously [62]. Briefly, glass
524 coverslips containing cells of interest were washed in PBS and fixed with either 4% paraformalde-
525 hyde (PFA) solution for 15 min at room temperature or on ice, or with ice-cold methanol for 10-12
526 min at -20 ºC. After three washes in PBS the PFA-fixed cells were permeabilized 10 min in 0.2%
527 Triton X-100 and 1% Bovine Serum Albumin (BSA) in PBS and blocked in 2% BSA in PBS for 1

528 hour at room temperature. Coverslips were incubated overnight at 4 ºC in primary antibodies (see
529 Key Resources Table) diluted in 2% BSA in PBS. The next day, coverslips were washed three
530 times with PBS for 5 min and incubated for 1 hour at room temperature in secondary antibodies
531 (see Key Resources Table) diluted in 2% BSA in PBS. Coverslips were washed three times in PBS
532 for 5 min before staining with 2 µg/ml DAPI solution PBS for 30 sec. Finally, coverslips were
533 washed once with PBS and before mounting on objective glass with 6% n-propyl gallate diluted in
534 glycerol and 10x PBS and combined with Shandon™ Immuno-Mount™ (Thermo Scientific, cat#
535 9990402) in a 1:12 ratio. Cells were imaged on a motorized Olympus BX63 upright microscope
536 equipped with a DP72 color, 12.8 megapixel, 4140 x 3096 resolution camera. cellSense Dimension
537 software 1.18 from Olympus was used to measure cilia length; ImageJ version 2.0.0-rc-69/1.52i
538 was used to measure the relative mean fluorescence intensity (MFI) of relevant antibody-labeled
539 antigens at the centrosome/basal body. A fixed circle was drawn around a centrosome in a cell. This
540 same region of interest (ROI) was used to measure the MFI of a specific protein at the centrosome.
541 A constant ROI was also drawn to measure the cell background signal which was subtracted from
542 the MFI measured at the centrosome/basal body. Images were prepared for publication using Adobe
543 Photoshop® and Adobe Illustrator®.
544 Super resolution imaging of RPE1 cells was conducted as described in [51] except that cells
545 were mounted in ProLong Diamond Antifade mountant. Settings for hardware-assisted axial and
546 software-assisted lateral channel alignment and image reconstruction were validated by imaging of
547 RPE1 cells stained for CEP164 and labeled with secondary antibodies conjugated to either
548 Alexa488, DyeLight550, or Alexa647. For superimposing 3D-SIM images on electron microscopy
549 micrographs of centrioles (kindly provided by Dr. Michel Bornens; [40]), 3D-SIM images were
550 sized to same digital pixel resolution as original EM images using the bicubic algorithm in ImageJ
551 and maximal intensity z-projections of single channel images overlaid on micrographs using centri-
552 ole centers / centriole distal ends as reference points.
553
554 **Statistical analysis**
555 Statistical analyses were performed using GraphPad Prism 6.0. The background-corrected MFI
556 measured at the centrosome was normalized to relevant control cells. Mean and standard deviation
557 (SD) was calculated for all groups, and outliers were identified and removed by the ROUT method
558 before the statistical tests were conducted. The data was tested for gaussian normality using either
559 D'Agostino's K-squared test or Shapiro-Wilk test. Depending on the distribution of the data, two-

560 tailed and unpaired Student's t-test or Mann Whitney test were used when comparing two groups.
561 Also, depending on the distribution of the data, One-way ANOVA followed by Tukey's, Dunnet´s
562 or Dunn's multiple comparison tests was used when comparing more than two groups. Unless oth-
563 erwise stated, the statistical analyses were performed on at least three independent biological repli-
564 cates (n=3). A p-value under 0.05 was considered statistically significant and p-values are indicated
565 in the figures with asterisks as follows; * $p<0.05$, ** <p0.01, ***<0.001, and **** $p<0.0001$.
566
567 **Immunoprecipitation (IP), protein quantification, SDS-PAGE and western blot analysis**
568 Immunoprecipitation of transfected 293T cell lysates was performed as described previously [61]
569 using relevant antibody-conjugated beads (see Key Resources Table). Protein concentrations were
570 measured using the *DC*™ Protein Assay Kit I from Bio-Rad (cat # 5000111) by following the man-
571 ufacturer's protocol. For SDS-PAGE analysis of RPE1 and HSF cells, protein samples were pre-
572 pared by lysis of cells with 95 ºC SDS-lysis buffer (1% SDS, 10 mM Tris-HCl, pH 7.4) and cell ly-
573 sates transferred to Eppendorf tubes and heated shortly at 95 ºC. The samples were then sonicated
574 two times for 30 seconds to shear DNA followed by centrifugation at 20,000 x *g* for 15 min at room
575 temperature to pellet cell debris. Supernatants were transferred to new Eppendorf tubes and an ali-
576 quot of each sample used for determination of protein concentration. Samples with equal concentra-
577 tions of protein were prepared for SDS-PAGE analysis by addition of NuPAGE™ LDS Sample
578 Buffer (4X) from Thermo Fisher Scientific (cat# NP0007) and 50 mM DTT. Samples from IP anal-
579 ysis in 293T cells, performed using modified EBC buffer [61], were prepared for SDS-PAGE in a
580 similar fashion. Protein samples were heated at 95 ºC for 5 minutes before loading them on a Mini-
581 PROTEAN® TGX™ Precast Gel 4-15% from Bio-Rab Laboratories, Inc. (cat# 456-1083 or cat
582 #456-1086). PageRuler™ Plus Prestained Protein Ladder (Thermo Fisher Scientific, cat# 26619)
583 was used as molecular mass marker. SDS-PAGE was performed using the Mini-PROTEAN® Tetra
584 System from Bio-Rad. Gels were run at 100 V for 15 minutes and 200 V for 45 minutes. Using the
585 Trans-BLOT® Turbo Transfer System from Bio-Rad Laboratories, Inc. the proteins were trans-
586 ferred at 1.3 A, 25 V for 10 min from the gel to a Trans-Blot® Turbo™ Transfer Pack, Mini format
587 0.2 µm Nitrocellulose membrane (cat# 1704158). Ponceau-S solution was added to the membrane
588 to visualize the proteins before blocking in 5% milk in Tris-buffered saline with Tween-20 (TBS-T;
589 10 mM Tris-HCl, pH 7.5, 150 mM NaCl, 0.1% Tween-20) for 2 hours at room temperature. Pri-
590 mary antibodies (see Key Resources Table) were diluted in 5% milk in TBS-T and incubated with
591 the membrane overnight at 4ºC. The membrane was washed three times 10 min at room temperature

592 in TBS-T on a shaker before incubation with secondary antibody (see Key Resources Table), di-
593 luted in 5% milk in TBS-T, for 1 hour at room temperature. The membrane was washed three times
594 10 min at room temperature in TBS-T on a shaker. Finally, SuperSignal™ west Pico PLUS chemi-
595 luminescent Substrate (Thermo Scientific, cat # 34580) was mixed in a 1:1 ratio and added to the
596 membrane for 5 min before development on a FUSION FX SPECTRA machine from Vilber.
597
598 **Quantitative mass spectrometry (MS) and peptide identification**
599 For SILAC-based mass spectrometry, three distinct SILAC culture media were used: light- (Lys0
600 and Arg0); medium- (Lys4 and Arg6) and high-labeled media (Lys8 and Arg10). 293T cells were
601 seeded in 100 mm petri dishes and SILAC labeled for 1 week to ensure proper amino acid incorpo-
602 ration. After the incorporation phase, the cells were transfected with 2 µg of plasmid encoding
603 FLAG-Ap80 (control), FLAG-CEP78 or FLAG-CEP78^{L150S} using 6 µl FuGENE®6, as described
604 above, and then subjected to lysis using modified EBC buffer [56] and FLAG IP as described
605 above. Affinity enriched proteins were digested with trypsin and the resulting peptides desalted
606 prior to LCMS analysis using an Easy-nLC 1000 system (Thermo Scientific) connected to a Q Ex-
607 active HF-X mass spectrometer (Thermo Scientific). Peptides were separated by a 70 minutes gra-
608 dient using increased buffer B (95% ACN, 0.5% acetic acid). The instrument was running in posi-
609 tive ion mode with MS resolution set at 60,000 for a scan range of 300 to 1700 m/z. Precursors
610 were fragmented by higher-energy collisional dissociation (HCD) with normalized collisional en-
611 ergy of 28 eV. For protein identification and quantitation, the obtained MS raw files were processed
612 by MaxQuant software version 1.6.1.0 [60] and searched against a FASTA file from UniProt.
613
614 **RNAseq analysis**
615 RNA was extracted using the Direct-zol RNA Miniprep Kit (Zymo Research) following the manu-
616 facturer's instructions. RNA degradation and contamination were monitored on 1% agarose gels.
617 RNA purity was checked using the NanoPhotometer® spectrophotometer (IMPLEN, CA, USA).
618 RNA concentration was measured using Invitrogen™ Qubit® RNA Assay Kit in Qubit® 2.0 Fluo-
619 rometer (Thermo Fisher Scientific). RNA integrity was assessed using the Agilent RNA Nano 6000
620 Assay Kit of the Bioanalyzer 2100 system (Agilent, CA, USA). A total amount of 3 µg RNA per
621 sample was used as input material for the RNA sample preparations. Sequencing libraries were gen-
622 erated using NEBNext® Ultra™ RNA Library Prep Kit for Illumina® (New England BioLabs,
623 USA) following manufacturer's recommendations and index codes were added to attribute

624 sequences to each sample. Briefly, mRNA was purified from total RNA using poly-T oligo-attached
625 magnetic beads. Fragmentation was carried out using divalent cations under elevated temperature in
626 NEBNext First Strand Synthesis Reaction Buffer（5X). First strand cDNA was synthesized using
627 random hexamer primer and M-MuLV Reverse Transcriptase（RNase H -）. Second strand cDNA
628 synthesis was subsequently performed using DNA Polymerase I and RNase H. Remaining over-
629 hangs were converted into blunt ends via exonuclease/polymerase activities. After adenylation of 3'
630 ends of DNA fragments, NEBNext Adaptor with hairpin loop structure were ligated to prepare for
631 hybridization. In order to select cDNA fragments of preferentially 150~200 bp in length, the library
632 fragments were purified with AMPure XP system (Beckman Coulter Life Sciences). Then 3 μl
633 USER® Enzyme (New England BioLabs) was used with size-selected, adaptor-ligated cDNA at
634 37°C for 15 min followed by 5 min at 95 °C before PCR. Then PCR was performed with Phusion®
635 High-Fidelity DNA polymerase, Universal PCR primers and Index (X) Primer (New England Bi-
636 oLabs). At last, PCR products were purified (AMPure XP system) and library quality was assessed
637 on the Agilent Bioanalyzer 2100 system. The clustering of the index-coded samples was performed
638 on a cBot Cluster Generation System using HiSeq PE Cluster Kit cBot-HS (Illumina) according to
639 the manufacturer's instructions. After cluster generation, the library preparations were sequenced on
640 an Illumina Hiseq platform and 125 bp/150 bp paired-end reads were generated. Raw data (raw
641 reads) of fastq format were firstly processed through in-house perl scripts. In this step, clean data
642 (clean reads) were obtained by removing reads containing adapter, reads containing poly-N and low
643 quality reads from raw data. At the same time, Q20, Q30 and GC content the clean data were calcu-
644 lated. All the downstream analyses were based on the clean data with high quality. Reference ge-
645 nome and gene model annotation files were downloaded from genome website directly. Index of the
646 reference genome was built using Bowtie v2.2.3 [63] and paired-end clean reads were aligned to the
647 reference genome using TopHat v2.0.12 [64]. We selected TopHat as the mapping tool for that
648 TopHat can generate a database of splice junctions based on the gene model annotation file and thus
649 a better mapping result than other non-splice mapping tools. HTSeq v0.6.1 [65] was used to count
650 the reads numbers mapped to each gene and then Fragments Per Kilobase of transcript sequence per
651 Millions base pairs sequenced (FPKM) of each gene was calculated based on the length of the gene
652 and reads count mapped to this gene. FPKM considers the effect of sequencing depth and gene
653 length for the reads count at the same time, and is currently the most commonly used method for
654 estimating gene expression levels [66]. Prior to differential gene expression analysis, for each se-
655 quenced library, the read counts were adjusted by edgeR program package through one scaling

656 normalized factor [67]. Differential expression analysis of two conditions was performed using the
657 DEGSeq R package (1.20.0) [68].
658
659 **Acknowledgements**
660 We thank Søren Lek Johansen and Maria Schrøder Holm for expert technical assistance, Benedicte
661 Schultz Kappel and Frida Roikjer Rasmussen for help with plasmid generation, and Nynne Chris-
662 tensen, Center for Advanced Bioimaging (CAB) Denmark, for help with 3D-SIM acquisition. Dr.
663 Kay Schink kindly provided plasmids for lentivirus particle generation and assisted in 3D-SIM ac-
664 quisition at OUH Radiumhospitalet. We are grateful to Drs. Peter K. Jackson, Tomoharu Kanie,
665 Francesc Garcia-Gonzalo, Laurence Pelletier, Brian David Dynlacht, Anne-Marie Tassin, Maria
666 Gavilan, Rosa M. Rios, Éric A. Cohen and Peter ten Dijke for reagents, and Dr. Michel Bornens for
667 sharing original EM microcraphs. This study was supported grants from Independent Research
668 Fund Denmark (#8020-00162B to PF and LBP, and #8021-00425A to JSA), from the Carlsberg
669 Foundation (#CF18-0294 to LBP) and from the Swiss National Science Foundation (#176097 to
670 CR).
671
672 **Figure legends**
673
674 **Figure 1.** CEP78 mutant cells display fewer, but longer primary cilia. (**A**) Representative IFM im-
675 ages of serum-deprived RPE1 WT and *CEP78* KO cells stained with the indicated antibodies; DAPI
676 marks the nucleus. Scale bar, 5μm. (**B**, **C**) Quantification of the percentage of ciliated cells (**B)** and
677 the length of residual cilia (**C)** in WT and *CEP78* KO cells, based on images as shown in (A). Data
678 were normalized in relation to WT values. Student's t-test (two-tailed, unpaired) was used for the
679 statistical analysis. Graphs in (B) represent accumulated data from three individual experiments
680 (n=384 for WT and n=322 for *CEP78* KO cells). Graphs in (C) show data from three individual ex-
681 periments (n=338 for WT and n=198 for *CEP78* KO cells). (**D**) Representative IFM images of se-
682 rum-deprived control and *CEP78* mutant (Patient) HSFs stained with the indicated antibodies;
683 DAPI marks the nucleus. Scale bar, 5 μm. (**E**, **F**) Quantification of the percentage of ciliated cells
684 (**E**) and the length of residual cilia (**F**) in control and *CEP78* patient HSFs (data from HSFs derived
685 from patient 2702r34, individual II-3 [29]), based on images as shown in (D). Graphs in (E) repre-
686 sent accumulated data from seven individual experiments (n= 678 for control HSFs; n= 707 for pa-
687 tient-derived HSFs). Graphs in (F) show data from seven individual experiments (n= 237 for

688 control HSFs; n= 216 for patient-derived HSFs). Data were normalized in relation to control values.
689 A Student's t-test (unpaired, two-tailed) was performed to address differences in the ciliary fre-
690 quency and length between control and patient HSFs. (**G**) Western blot analysis of Rb phosphory-
691 lated on S807/811 (P-Rb) in RPE1 WT and *CEP78* KO cells grown with or without serum. (**H**, **I**)
692 Quantification of data shown in (G) from three independent experiments analyzed in duplicates. (**J**)
693 P-Rb blots from HSFs derived from control and patient HSFs grown with or without serum (data
694 from HSFs derived from patient F3: II:1; [30]). GAPDH was used as a loading control. (**K, L**)
695 Quantification of data shown in (J) from three independent experiments analyzed in duplicates. Stu-
696 dent's t-test (two-tailed, unpaired) was used for the statistical analysis in (H, I) and (K, L). Error
697 bars of graphs represent SD and data are shown as mean ± SD. a.u., arbitrary units; (*) $p<0.05$;
698 (****) $p<0.0001$; n.s., not statistically significant.
699
700 **Figure 2.** Analysis of RPE1 WT and *CEP78* KO cells expressing FLAG- or mNG-tagged CEP78 or
701 CEP78^{L150S} fusions. (**A**) Representative IFM images of serum-starved WT and *CEP78* KO cells
702 transiently expressing FLAG-CEP78 and FLAG-CEP78^{L150S} labeled with antibodies against FLAG
703 (green) and ARL13B (magenta). Insets show enlarged views of the cilia-centrosome region. Scale
704 bars: 5 μm in original images and 1 μm in magnified images. (**B**) Quantification of the relative MFI
705 of FLAG-CEP78 and FLAG-CEP78^{L150S} at the centrosome in serum-starved WT cells. Accumu-
706 lated data from three individual experiments (n=145 and n=151 for cells transfected with FLAG-
707 CEP78 and FLAG-CEP78^{L150S}, respectively). Student's t-test (two-tailed, unpaired) was used for
708 the statistical analysis. Data is shown as mean ±SD. (**C, D**). Quantification of the percentage of cili-
709 ated cells (**C**) or ciliary length (**D**) in serum-deprived WT and *CEP78* KO cells stably expressing
710 mNG-CEP78 or mNG-CEP78^{L150S}. Analysis on cilia numbers and length was performed through
711 accumulated data from three independent experiments for WT, *CEP78* KO and WT + mNG-CEP78
712 cells and five independent experiments for *CEP78* KO cells expressing either the mNG-CEP78 or
713 the mNG-CEP78^{L150S} (for ciliary frequency: n=304 for WT; n=322 for *CEP78* KO; n=425 for WT
714 + mNG-CEP78; n=621 for C*EP78* KO + mNG-CEP78, and n=638 for C*EP78* KO + mNG-
715 CEP78^{L150S}; for ciliary length: n=145 for WT; n=56 for *CEP78* KO; n=138 for WT + mNG-
716 CEP78; n=280 for C*EP78* KO + mNG-CEP78 and n=141 for C*EP78* KO + mNG-CEP78^{L150S}). Or-
717 dinary one-way ANOVA with Dunnett's multiple comparison test was used for the statistical analy-
718 sis of the ciliary frequency and length amongst all groups, in relation to the mean of WT cells, des-
719 ignated as the control group. Differences between *CEP78* KO and *CEP78* KO+ mNG-CEP78;

720 *CEP78* KO and *CEP78* KO + mNG-CEP78^{L150S} and *CEP78* KO + mNG-CEP78 and *CEP78* KO +
721 mNG-CEP78^{L150S} were addressed in a pairwise fashion using an unpaired and two-tailed Student´s
722 t-test. Error bars in (C) indicate SD and data in (D) is presented as mean ± SD. (*) $p<0.05$; (**)
723 $p<0.01$; (***) $p<0.001$; (****) $p<0.0001$; n.s, not statistically significant; a.u., arbitrary units.
724
725 **Figure 3.** CEP78 interacts with the EDD-DYRK2-DDB1^{VPRBP} complex and CEP350. (**A**) Overview
726 of results from CEP78 interactome analysis in 293T cells grown in SILAC medium. Cells expressing
727 FLAG-CEP78 WT, FLAG-CEP78^{L150S} or FLAG-Ap80 (negative control) were subjected to FLAG
728 IP and pellets analyzed by mass spectrometry. The upper panel displays affinity enrichment of Cep78
729 and interaction partners in FLAG-CEP78 WT cells relative to control cells. The lower panel shows
730 how the CEP78^{L150S} mutation weakens these interactions relative to CEP78 WT using ratios normal-
731 ized for equal affinity enrichment of FLAG-tagged CEP78. (**B-D**) 293T cells expressing the indicated
732 Myc-, FLAG-, or GFP-fusions were subjected to IP with anti-FLAG (**B**) or -GFP (**C**, **D**) beads and
733 input and pellet fractions analyzed by SDS-PAGE and western blotting with Myc, FLAG or GFP
734 antibodies as indicated. FLAG-Ap80-NB used in (B) is a negative control. Molecular mass markers
735 are indicated in kDa to the left of the blots. (**E**) Schematic of the CEP350 and CEP78 fusions used in
736 IP analysis. LRR, leucine-rich repeat; CC, coiled coil. The CEP350 constructs were described in [54,
737 58]; the CEP78 constructs were generated in this study based on published sequence information [27,
738 30, 35]. N, N-terminal region; M, middle region; NM, N-terminal plus middle region; C, C-terminal
739 region; FL, full length.
740
741 **Figure 4.** CEP350 regulates stability and centrosomal recruitment of CEP78. (**A**) 3D-SIM analysis
742 of mNG-CEP78 and CEP350 localization in WT RPE1 cells, relative to CP110 and CEP164 (maxi-
743 mal z-projections). Cells were fixed and stained with the indicated antibodies. Montage panels show
744 single channel images of the mother centriole region (left panels) and overlays on previously pub-
745 lished electron micrographs of isolated mother centrioles from KE37 cells, reproduced with permis-
746 sion from [40] (top: cross-sections of proximal and subdistal-appendage region; bottom: side-view).
747 Scale bar, 200 nm. (**B**) Western blot analysis of CEP78 and α-tubulin (loading control) in serum-
748 deprived hTERT-RPE1-BFP-Cas9 control (pMCB306), *CEP350* KO or *FOP* KO cells [24]. (**C**)
749 Quantification of data in (B), based on three independent experiments analyzed in duplicates. Error
750 bars indicate SD. Statistical analysis was done using Student's t-test (unpaired, two-tailed). (**D, F**)
751 IFM analysis of serum-deprived control and *CEP350* KO ciliated (D) and non-ciliated cells (F)

752 using antibodies as indicated. Dashed boxes indicate cropped images to highlight the centro-
753 somal/ciliary area. Scale bars: 5 µm in representative images and 1 µm in insets. (**E, G**) Quantifica-
754 tion of the relative MFI of CEP78 at the centrosome in serum-starved, ciliated (E) and non-ciliated
755 (G) control and *CEP350* KO cells, based on images as shown in (D) and (F), respectively. Statisti-
756 cal analysis was done using a two-tailed and unpaired Mann-Whitney test for ciliated cells and two-
757 tailed and unpaired Student's t-test for non-ciliated cells. Accumulated data from three individual
758 experiments (n=128 and 132 for control and *CEP350* KO ciliated cells, respectively; n= 101 and
759 107 for control and *CEP350* KO non-ciliated cells, respectively). a.u., arbitrary units; (*) $p<0.05$;
760 (**) $p<0.01$; (****) $p<0.0001$.
761
762 **Figure 5.** Altered centrosomal levels of CEP350 in *CEP78* mutant cells. (**A, C, E, G**) Representa-
763 tive IFM images of ciliated (**A**) and non-ciliated (**C**) serum-deprived RPE1 WT and *CEP78* KO
764 cells, and ciliated (**E**) and non-ciliated (**G**) serum-deprived control and CEP78 deficient (Patient)
765 HSFs (combined data from HSFs from patient F3: II:1 [30] and patient 2702r34, individual II-3
766 [29]) labeled with antibodies indicated in the figure. Insets show closeups of the centrosomal/ciliary
767 area (dashed boxes). Scale bars: 5 µm in representative images and 1 µm in closeups. (**B, D**). Quan-
768 tification of CEP350 relative MFI at the centrosome based on images as shown in (A, C). Data is
769 shown as mean ± SD. A Student's t-test was used as statistical analysis between the two groups
770 based on three individual experiments (n=157 or 158 for ciliated cells and n=144-152 for non-cili-
771 ated cells). (**F, H)** Quantification of CEP350 relative MFI at the centrosome in HSFs based on im-
772 ages as shown in (E, G). Data is shown as mean ± SD. Student's t-test was used as statistical analy-
773 sis between the two cell groups based on seven individual experiments with a total of 154 and 156
774 analyzed ciliated cells (**F**), and three individual experiments with a total of 122 or 126 analyzed
775 non-ciliated cells (**H**). a. u., arbitrary units; n.s, not statistically significant; (****) $p<0.0001$.
776
777 **Figure 6.** Analysis of EDD-DYRK2-DDB1^{VPRBP} complex components in CEP78 deficient cells.
778 (**A**) Western blot analysis of VPRBP in lysates from serum-fed and serum-deprived RPE1 WT and
779 *CEP78* KO cells. α-tubulin was used as a loading control (**B, C**) Quantification of the VPRBP rela-
780 tive levels in the different conditions depicted in (A). Statistical analysis was performed using a
781 Student's t-test (unpaired, two-tailed) from five independent experiments analyzed in duplicates.
782 Error bars indicate SD. (**D, F)** Representative IFM images of ciliated (**D**) and non-ciliated (**F**) se-
783 rum-deprived RPE1 WT and *CEP78* KO cells labeled with antibodies against EDD1 (green) and

784 DCTN1 plus acetylated tubulin (magenta). DAPI was used to mark the nucleus (blue). Insets show
785 enlarged views of the cilium-centrosome region. Scale bars: 5 µm in original images and 1 µm in
786 closeups. (**E, G)** Quantification of the EDD1 MFI at the centrosome based on images as shown in
787 (D) and (F) using a two-tailed and unpaired Student's t-test. Data is shown as mean ± SD. Student's
788 t-test from three independent experiments (n=194 and n=201 for ciliated WT and *CEP78* KO cells,
789 respectively; n=194 and n=217 for non-ciliated WT and *CEP78* KO cells, respectively). Data is
790 shown as mean ± SD. a.u., arbitrary units; n.s., not statistically significant; (****) p<0.0001.
791
792 **Figure 7.** CEP78 deficient cells display elevated cellular and centrosomal levels of CP110. (**A**)
793 Western blot analysis of lysates from serum-deprived RPE1 WT and *CEP78* KO cells using indi-
794 cated antibodies. GAPDH was used as a loading control. (**B**) Quantification of the data shown in
795 (A), based on four independent experiments analyzed in duplicates. Error bars indicate SD. Statisti-
796 cal analysis was done using Student's t-test (unpaired, two-tailed). (**C, F**) Representative IFM im-
797 ages of serum-starved ciliated (**C**) and non-ciliated (**F**) RPE1 WT and *CEP78* KO cells labeled with
798 antibodies against CP110 (green), combined DCTN1 and acetylated tubulin (Ac-tub; magenta) and
799 DAPI to mark the nucleus (blue). Insets show enlarged views of the cilium-centrosome area. Scale
800 bars: 5 µm in original images and 1 µm in closeups. (**D, G**) Quantification of the relative MFI of
801 CP110 at the centrosome based on images as shown in (C) and (F), respectively. Student's t-test
802 (unpaired, two-tailed) from three independent biological experiments (n= 90 and n=75 for ciliated
803 RPE1 WT and *CEP78* KO cells, respectively; n=75 and n=82 for non-ciliated RPE1 WT and
804 CEP78 KO cells, respectively) was used for statistical analysis. Data is presented as mean ± SD. (**E**)
805 Quantification of the relative MFI of CP110 at the mother centriole based on images shown in (C)
806 Mann Whitney test (two-tailed and unpaired) was used as statistical analysis based on two inde-
807 pendent experiments (n=61 and n=62 for RPE1 WT and CEP78 KO cells, respectively). Data is
808 presented as mean ± SD. (**H**) Representative IFM images of serum-deprived healthy and CEP78 de-
809 ficient (Patient) HSFs (data from patient 2702r34, individual II-3 described in [29]) labeled with the
810 indicated antibodies. DAPI was used as counterstaining to mark the nucleus. Dashed lines show
811 closeup images of the centrosome region. Scale bars: 5 µm in original images and 1 µm in closeups.
812 (**I**) Quantification based on observations of 151 and 155 cells of CEP78 control and patient cells,
813 respectively, from three individual experiments. Student's t-test (unpaired and two-tailed) was used
814 to assess differences between the two groups. a.u., arbitrary units; n.s., not statistically significant;
815 (**) p<0.01; (***) p<0.001; (****) p<0.0001.

816

817 **Figure 8.** Depletion of CP110 from *CEP78* KO cells rescues their ciliation frequency phenotype.
818 (**A**) Representative western blots of RPE1 WT or *CEP78* KO cells treated with control (siMock) or
819 CP110-specific siRNA (siCP110). Cells were deprived of serum and blots were probed with anti-
820 body against CP110 or α-tubulin (loading control). (**B**) Quantification of relative cellular CP110
821 levels under different conditions based on blots as shown in (A) (n=5 for WT and n=4 for *CEP78*
822 KO cells; each sample was analyzed in duplicates). Error bars indicate SD. Data was normalized in
823 relation to the WT cells transfected with Mock siRNA (WT siMock), designated as the control
824 group. Differences of CP110 relative levels between *CEP78* KO cells transfected with Mock or
825 CP110 siRNA and WT cells transfected with CP110 siRNA in relation to control were assessed by
826 performing an ordinary one-way ANOVA with a Dunnet´s multiple comparison test. Differences of
827 CP110 cellular levels between *CEP78* KO cells transfected with the same siRNAs was addressed
828 using an unpaired and two-tailed Student's t-test. (**C**) Representative IFM images of serum-de-
829 prived RPE1 WT and *CEP78* KO cells treated with control (siMock) or CP110-specific siRNA
830 (siCP110) and stained for ARL13B (green). DAPI marks the nucleus. Dashed boxes indicate
831 cropped images to highlight the centrosomal/ciliary zone. Scale bars, 5 μm in representative images
832 and 1μm in insets. (**D**, **E**) Quantification of percentage of ciliated cells (**D**) and length of remaining
833 cilia (**E**) in RPE1 WT or *CEP78* KO cells treated with control (siMock) or CP110-specific siRNA
834 (siCP110). The quantification is based on images as shown in (C) and represents data from four and
835 five independent experiments, respectively, for RPE1 WT (n=554-617cells per condition) and
836 *CEP78* KO cells (n=846-856 cells per condition). Ordinary one-way ANOVA with Dunnett's mul-
837 tiple comparison test was used, to compare the mean of the remaining groups in relation with the
838 mean of RPE1 WT cells treated with siMock, which was designated as the control group. Differ-
839 ences between *CEP78* KO cells transfected with the above-mentioned siRNA were discriminated
840 using an unpaired and two-tailed Student´s t-test. Bars in (D) represent SD and data in (E) is pre-
841 sented as mean ± SD. a.u., arbitrary units; (*) $p<0.05$; (**) $p<0.01$; (***) $p<0.001$; (****)
842 $p<0.0001$. (**F**) Proposed model for how CEP78 regulates ciliogenesis and ciliary length control. See
843 text for details.

844

845 **Supplementary figure legends**

846

847 **Figure 1-figure supplement 1.** Western blot analysis and ciliary frequency and length in RPE1 WT
848 and *CEP78* KO clones. **(A)** Western blot analysis of serum-deprived RPE1 WT and four different
849 *CEP78* KO clones, generated by CRISPR/Cas9 methodology. Blots were probed with antibodies
850 against CEP78 and GAPDH (loading control), as indicated. The lower band in the CEP78 blot is
851 due to unspecific staining of the antibody. Molecular mass markers are indicated in kDa to the right.
852 Unless otherwise indicated, clone #73 was used for all experiments in RPE1 cells performed in this
853 manuscript, and is designated *CEP78* KO. (**B, C**) Quantification of ciliary frequency (B) and length
854 (C) in serum-deprived RPE1 WT and different *CEP78* KO clones. Differences in cilia numbers and
855 size between the WT and the several *CEP78* KO clones were addressed through accumulated data
856 from three independent experiments (for cilia frequency: n= 304 for WT; n=308 for clone #2;
857 n=321 for clone #44 and n=311 for clone #52; and for ciliary length: n=145 for WT; n=68 for clone
858 #2; n=98 for clone #44 and n=62 for clone #52) by performing an ordinary one-way ANOVA with
859 Dunnet´s multiple comparison test amongst all groups, in relation to WT cells mean (control
860 group). Error bars in (B, C) indicate mean ± SD. (*) $p<0.05$; (**) $p<0.01$; (***) $p<0.001$.
861
862 **Figure 2-figure supplement 1.** Expression of FLAG-CEP78 and FLAG-CEP78^{L150S} in RPE1 WT
863 and *CEP78 KO* cells. **(A)** FLAG blots from serum-deprived WT and *CEP78* KO lysates transfected
864 with indicated FLAG fusions. GAPH was used as a loading control. (**B**) Quantification of data de-
865 picted in (A). Graphs of the FLAG blots are presented as the mean + SD from three individual ex-
866 periments analyzed in duplicates. Ordinary one-way ANOVA with Tukey's multiple comparison
867 test was used for the statistical analysis, where no significant statistical differences were reported
868 between the groups.
869
870 **Figure 2-figure supplement 2.** CEP78 endogenous antibody binds equally well to FLAG-CEP78
871 WT and L150S mutant fusions. 293T cells transiently expressing FLAG-CEP78 or FLAG-
872 CEP78^{L150S} were subjected to IP with FLAG. Pellet fractions were analyzed by SDS-PAGE and
873 western blotting using antibodies against FLAG and endogenous CEP78. Molecular mass marker is
874 indicated in kDa to the left of the blots.
875
876 **Figure 2-figure supplement 3.** Stable expression of mNG-CEP78 and mNG-CEP78^{L150S} in RPE1
877 WT and *CEP78* KO cells. **(A)** Western blots of lysates of serum-deprived WT and *CEP78* KO
878 RPE1 cells lines stably expressing the indicated mNG-tagged fusions. The blots were probed with

879 antibodies against CEP78 (upper panel) and α-tubulin (loading control; lower panel). Molecular
880 mass markers are shown in kDa to the left. (**B**) Representative light (upper panels) and fluorescence
881 (lower panels) images of live cells expressing the indicated fusions. Note that mNG-CEP78 is con-
882 centrated at the centrosome whereas mNG-CEP78^{L150S} is not. Scale bar, 20 μm.
883
884 **Figure 3-figure supplement 1.** CEP78 associates independently with CEP350 and VPRBP. (**A**)
885 293T cells expressing the indicated Myc- or GFP-fusions were subjected to IP with Myc antibody-
886 coated beads and input and pellet (IP Myc) fractions analyzed by SDS-PAGE and western blotting
887 with VPRBP, Myc, FOP or GFP antibodies as indicated. (**B**) Similar analysis as in (A), but using
888 GFP antibody-coated beads for IP instead of Myc beads. Molecular mass markers are indicated in
889 kDa to the left of the blots. Arrowhead in (A) indicates IgG band observed in the lower part of the
890 GFP blot.
891
892 **Figure 4-figure supplement 1.** Validation of *CEP350* KO cells by IFM analysis. (**A**) RPE1 control
893 and *CEP350* KO cells were serum starved for 24 hours before fixation and staining with the indi-
894 cated antibodies and DAPI for nuclear visualization. Insets show closeups of the centrosomal/ciliary
895 area (dashed boxes). Scale bars: 5 μm in representative images and 1 μm in closeups. (**B**) Quantifi-
896 cation of CEP350 mean fluorescence intensity (MFI) at the centrosome, based on images as shown
897 in (A). A total of 38 and 26 cells were analyzed for control and *CEP350* KO cells, respectively. For
898 statistical analysis, the data was first normalized to the control group values and differences were
899 assessed using an unpaired and two-tailed Student´s t-test. Data is shown as the mean ± SD. a.u.,
900 arbitrary units; (**) $p<0.01$.
901
902 **Figure 6-figure supplement 1.** VPRBP centrosomal levels are increased or unchanged in RPE1
903 *CEP78* KO cells. (**A, C**) Representative IFM micrographs of ciliated (**A**) and non-ciliated (**C**) se-
904 rum-starved RPE1 WT and *CEP78* KO cells labeled with the antibodies indicated in the figure.
905 DAPI was used to mark the nucleus (blue). Insets show enlarged views of the cilium-centrosome
906 region. Scale bars: 5 μm in original images and 1 μm in closeups. (**B, D**) Quantification of the
907 VPRBP MFI at the centrosome based on images shown in (A) and (C) based on data from three in-
908 dependent experiments (n= 156 and n=158 for ciliated WT and CEP78 KO cells, respectively; n=
909 162 and n= 166 for non-ciliated WT and CEP78 KO cells, respectively) using a two-tailed and

910 unpaired Student's t-test. Data is shown as mean ± SD and was first normalized in relation to WT
911 values. a.u., arbitrary units; (**) $p<0.01$; n.s., not statistically significant.
912
913 **Figure 6-figure supplement 2.** EDD1 centrosomal levels are reduced in RPE1 *CEP350* KO cells.
914 (**A, C**) Representative IFM micrographs of ciliated (**A**) and non-ciliated (**C**) serum-starved RPE1
915 control and *CEP350* KO cells labeled with the antibodies indicated in the figure. DAPI was used to
916 mark the nucleus (blue). Insets show enlarged views of the cilium-centrosome region. Scale bars: 5
917 μm in original images and 1 μm in closeups. (**B, D**) Quantification of the EDD1 MFI at the centro-
918 some based on images as shown in (A) and (C) using a two-tailed and unpaired Student´s t-test
919 from two independent experiments (n=105 and n= 111 for ciliated WT and *CEP78* KO cells, re-
920 spectively; n=118 for non-ciliated WT and CEP78 KO cells). Data is shown as mean ± SD and was
921 first normalized in relation to WT values. a.u., arbitrary units; (****) $p<0.0001$.
922
923 **Figure 7-figure supplement 1.** Elevated cellular CP110 levels in RPE1 *CEP78* KO clones. **(A)**
924 Western blot analysis of serum deprived RPE1 WT and three different *CEP78* KO clones, as indi-
925 cated. Blots were probed with antibodies against CP110 and GAPDH (loading control). Molecular
926 mass markers are indicated in kDa to the right. (**B**) Quantification of relative cellular CP110 levels
927 based on blots as shown in (A) from two independent experiments. The means of the CEP78 KO
928 clones, were compared in relation to the WT mean, selected as the control group using an ordinary
929 one-way ANOVA followed by a Dunnet´s multiple comparison test. Error bars of graphs represent
930 SD and data are shown as mean ± SD. (**C**) Representative western blot of WT and *CEP78* KO cells
931 (KO; clone #73) stably expressing mNG-CEP78 or mNG-CEP78^{L150S} as indicated. Blots were
932 probed with indicated antibodies (α-tub=α-tubulin) and the molecular mass markers are indicated
933 in kDa to the right of the blot. Quantification of relative CP110 band intensities revealed no signifi-
934 cant changes between the three conditions; CP110 level relative to that of WT mNG-CEP78 was
935 95% +/-12% for the *CEP78* KO mNG-CEP78 line and 90% +/- 9% for the *CEP78* KO mNG-
936 CEP78^{L150S} line, respectively (n=3). Blots were probed with indicated antibodies.
937
938 **Figure 7-figure supplement 2.** Serum-fed CEP78 deficient cells display elevated cellular and cen-
939 trosomal levels of CP110. (**A**) CP110 western blot analysis of lysates from RPE1 WT and *CEP78*
940 KO cells grown in the presence of serum; α-tubulin serves as loading control. (**B**) Quantification of
941 the CP110 blots depicted in (A) based on four individual experiments analyzed in duplicates. Error

942 bars indicate SD. Student's t-test (unpaired, two-tailed) was used to analyze the differences between
943 both cellular groups. (**C**) Representative IFM images of cycling RPE1 WT and *CEP78* KO cells la-
944 beled with the indicated antibodies. DAPI was used to mark the nucleus. Insets show closeup im-
945 ages of the centrosome region. Scale bars: 5 µm in original images and 1 µm in closeups. (**D**) Data
946 quantification of the relative MFI of CP110 based on images as shown in (C). Data is present as
947 mean ±SD. Statistical analysis was performed using Student's t-test (unpaired, two-tailed) of three
948 independent experiments (n=158 for WT and n= 147 for *CEP78* KO cells). a.u., arbitrary units; (*)
949 $p<0.05$; (****) $p<0.0001$.
950
951 **Figure 7-figure supplement 3.** Barplots showing expression of *CP110, CEP350,*
952 *VRPBP* and *EDD1* genes for patients (n=3) and controls (n=4), based on RNA-seq data of skin fi-
953 broblasts. Expression levels are shown in fpkm (Fragments Per Kilobase of transcript sequence per
954 Millions base pairs sequenced). The patient data are combined data from HSFs derived from three
955 different *CEP78* probands; F3 individual II:1 described in [30] and KN10 individual II-1 and
956 2716s15 individual II-2 described in [29]. Control data are combined data from HSFs from four un-
957 affected individuals described in the same studies. Nominal p-values derived from unpaired two-
958 tailed t-tests are shown on top of the bars. None of the comparisons were significantly different
959 ($p<0.05$).
960
961 **Figure 7-figure supplement 4.** Relative CP110 levels in WT and *CEP78* KO cells treated with cy-
962 cloheximide. (**A**) Representative western blot of lysates from serum-deprived WT and *CEP78* KO
963 cells treated with 200 ng/ml cycloheximide (CHX) for the indicated times. The drug was added at
964 the onset of serum deprivation (time 0 h). Blots were probed with CP110 and GAPDH (loading
965 control) antibodies; molecular mass markers are shown in kDa to the left. (**B**) Quantification of av-
966 erage CP110 levels determined based on western blots as shown in (A). The analysis is based on
967 data from four independent experiments, normalized to the relative CP110 level for each cell type at
968 time zero. Note that the data indicates decline in CP110 levels with time in the WT cells but not in
969 the *CEP78* KO cells; however, due to fluctuations from experiment to experiment the changes were
970 not statistically significant (ns; p values denoted in parenthesis above the graphs). The data is pre-
971 sented as mean ±SD.
972

973 **Figure 8-figure supplement 1.** Validation of CP110 knockdown in RPE1 WT and *CEP78* KO
974 cells by IFM. (A, B) Quantification of CP110 centrosomal levels in ciliated and non-ciliated WT
975 and *CEP78* KO cells treated with control (siMock) or CP110-specific siRNA (siCP110). Both
976 graphs are based on one biological experiment with 35 observations of ciliated and 35 observations
977 of non-ciliated cells per condition. Statistical analysis was performed using and Ordinary One-way
978 ANOVA followed by a Dunnett´s multiple comparison test amongst all groups in relation to WT
979 siMock, designated as the control group. Differences between *CEP78* KO cells treated with siMock
980 or siCP110 were addressed by performing an unpaired and two-tailed Student´s t-test. Bars are rep-
981 resented as mean ±SD. (a.u.) arbitrary units; (*) $p<0.05$; (**) $p<0.01$.
982
983 **Additional files**
984 **Figure 1-source data 1.** Original western blots corresponding to Figure 1G. The upper blots are la-
985 beled with pRb antibody and lower blots with GAPDH antibody.
986 **Figure 1-source data 2.** Original western blots corresponding to Figure 1J. The upper blots are la-
987 beled with pRb antibody and lower blots with GAPDH antibody.
988 **Figure 3-source data 1.** Raw data from the CEP78 interactome analysis depicted in Figure 3A.
989 293T cells grown in SILAC medium and expressing FLAG-CEP78 WT, FLAG-CEP78^{L150S} or
990 FLAG-Ap80 (negative control) were subjected to FLAG IP and pellets analyzed by mass spectrom-
991 etry.
992 **Figure 3-source data 2.** Original western blots corresponding to Figure 3B. Upper left, input Myc
993 blot; upper middle, input 100 kDa FLAG blot; upper right, IP Myc and 100 kDa FLAG blots; bot-
994 tom left, input 35 kDa FLAG blot; bottom right, IP 35 kDa FLAG blot.
995 **Figure 3-source data 3.** Original western blots corresponding to Figure 3C. Upper left, input Myc
996 blot; upper middle, IP Myc blot; upper right, input GFP blot; bottom left, IP GFP blot; bottom mid-
997 dle, inpot FOP blot; bottom right, IP FOP blot.
998 **Figure 3-source data 4.** Original western blots corresponding to Figure 3D. Upper left, input Myc
999 blot; upper right, IP Myc blot; lower left, input GFP blot; lower right, IP GFP blot.
1000 **Figure 4-source data 1.** Original western blots for Figure 4B. Left, CEP78 blot; right, α-tubulin
1001 blot.
1002 **Figure 6-source data 1.** Original western blots for Figure 6A. Left, VPRBP blot; right, α-tubulin
1003 blot.

1004 **Figure 7-source data 1.** Original western blots for Figure 7A. Left, CP110 blot; right, GAPDH
1005 blot.
1006 **Figure 8-source data 1.** Original bots for Figure 8A. Left, CP110 blot; right, α-tubulin blot.
1007 **Figure 1-figure supplement 1-source data 1.** Original western blots for Figure 1-figure supple-
1008 ment 1. Left, CEP78 blot; right, GAPDH blot.
1009 **Figure 2-figure supplement 1-source data 1.** Original western blots for Figure 2-figure supple-
1010 ment 1. Left, FLAG blot; right, GAPDH blot.
1011 **Figure 2-figure supplement 2-source data 1.** Original western blots for Figure 2-figure supple-
1012 ment 2. Left, FLAG blot; right, CEP78 blot.
1013 **Figure 2-figure supplement 3-source data 1.** Original western blots for Figure 2-figure supple-
1014 ment 3. Left, CEP78 blot; right, α-tubulin blot
1015 **Figure 3-figure supplement 1-source data 1.** Original western blots for Figure 3-figure supple-
1016 ment 1A. Top row from left to right: input VPRBP blot, IP VPRBP blot, input Myc blot. Second
1017 row from left to right: IP Myc blot, input FOP blot, IP FOP blot. Third row from left to right: input
1018 GFP blot (upper), IP GFP blot (upper). Fourth row left to right: input GFP blot (lower), IP GFP blot
1019 (lower).
1020 **Figure 3-figure supplement 1-source data 2.** Original western blots for Figure 3-figure supple-
1021 ment 1B. Top row, input VPRBP blot; second row, IP VPRBP blot; third row left, input Myc blot;
1022 third row right, IP Myc blot; fourth row left, input GFP blots; fourth row right, IP GFP blots.
1023 **Figure 7-figure supplement 1-source data 1.** Original western blots for Figure 7-figure supple-
1024 ment 1. Left, CP110 (upper) and GAPDH blots in panel A. Right, CP110 (upper) and α–tubulin
1025 (lower) blots in panel C.
1026 **Figure 7-figure supplement 2-source data 1.** Original western blots for Figure 7-figure supple-
1027 ment 2A. Top, CP110 blot; bottom, α–tubulin blot.
1028 **Figure 7-figure supplement 3-source data 1.** Raw RNA seq data for Figure 7-figure supplement
1029 3.
1030 **Figure 7-figure supplement 4-source data 1.** Original western blots for Figure 7-figure supple-
1031 ment 4A. Upper left, WT CP110 blot; upper right, WT GAPDH blot. Lower left, *CEP78* KO
1032 CP110 blot; lower right, *CEP78* KO GAPDH blot.
1033

1034 **References**

1035

1036 1. Anvarian, Z., K. Mykytyn, S. Mukhopadhyay, L.B. Pedersen, and S.T. Christensen, *Cellular*
1037 *signalling by primary cilia in development, organ function and disease.* Nat Rev Nephrol,
1038 2019. **15**(4): p. 199-219.
1039 2. Nachury, M.V. and D.U. Mick, *Establishing and regulating the composition of cilia for*
1040 *signal transduction.* Nat Rev Mol Cell Biol, 2019. **20**(7): p. 389-405.
1041 3. Reiter, J.F. and M.R. Leroux, *Genes and molecular pathways underpinning ciliopathies.* Nat
1042 Rev Mol Cell Biol, 2017. **18**(9): p. 533-547.
1043 4. Breslow, D.K. and A.J. Holland, *Mechanism and Regulation of Centriole and Cilium*
1044 *Biogenesis.* Annu Rev Biochem, 2019. **88**: p. 691-724.
1045 5. Spektor, A., W.Y. Tsang, D. Khoo, and B.D. Dynlacht, *Cep97 and CP110 suppress a cilia*
1046 *assembly program.* Cell, 2007. **130**(4): p. 678-90.
1047 6. Chen, Z., V.B. Indjeian, M. McManus, L. Wang, and B.D. Dynlacht, *CP110, a cell cycle-*
1048 *dependent CDK substrate, regulates centrosome duplication in human cells.* Dev Cell,
1049 2002. **3**(3): p. 339-50.
1050 7. Kleylein-Sohn, J., J. Westendorf, M. Le Clech, R. Habedanck, Y.D. Stierhof, and E.A.
1051 Nigg, *Plk4-induced centriole biogenesis in human cells.* Developmental cell, 2007. **13**(2): p.
1052 190-202.
1053 8. D'Angiolella, V., V. Donato, S. Vijayakumar, A. Saraf, L. Florens, M.P. Washburn*, et al.*,
1054 *SCF(Cyclin F) controls centrosome homeostasis and mitotic fidelity through CP110*
1055 *degradation.* Nature, 2010. **466**(7302): p. 138-42.
1056 9. Li, J., V. D'Angiolella, E.S. Seeley, S. Kim, T. Kobayashi, W. Fu*, et al.*, *USP33 regulates*
1057 *centrosome biogenesis via deubiquitination of the centriolar protein CP110.* Nature, 2013.
1058 **495**(7440): p. 255-9.
1059 10. Sorokin, S., *Centrioles and the formation of rudimentary cilia by fibroblasts and smooth*
1060 *muscle cells.* J Cell Biol, 1962. **15**: p. 363-377.
1061 11. Sorokin, S.P., *Reconstructions of centriole formation and ciliogenesis in mammalian lungs.*
1062 J Cell Sci, 1968. **3**(2): p. 207-30.
1063 12. Shakya, S. and C.J. Westlake, *Recent advances in understanding assembly of the primary*
1064 *cilium membrane.* Fac Rev, 2021. **10**: p. 16.
1065 13. Kobayashi, T., W.Y. Tsang, J. Li, W. Lane, and B.D. Dynlacht, *Centriolar kinesin Kif24*
1066 *interacts with CP110 to remodel microtubules and regulate ciliogenesis.* Cell, 2011. **145**(6):
1067 p. 914-25.
1068 14. Huang, N., D. Zhang, F. Li, P. Chai, S. Wang, J. Teng*, et al.*, *M-Phase Phosphoprotein 9*
1069 *regulates ciliogenesis by modulating CP110-CEP97 complex localization at the mother*
1070 *centriole.* Nat Commun, 2018. **9**(1): p. 4511.
1071 15. Cajanek, L. and E.A. Nigg, *Cep164 triggers ciliogenesis by recruiting Tau tubulin kinase 2*
1072 *to the mother centriole.* Proc Natl Acad Sci U S A, 2014. **111**(28): p. E2841-50.
1073 16. Oda, T., S. Chiba, T. Nagai, and K. Mizuno, *Binding to Cep164, but not EB1, is essential*
1074 *for centriolar localization of TTBK2 and its function in ciliogenesis.* Genes Cells, 2014.
1075 **19**(12): p. 927-40.
1076 17. Lo, C.H., I.H. Lin, T.T. Yang, Y.C. Huang, B.E. Tanos, P.C. Chou*, et al.*, *Phosphorylation*
1077 *of CEP83 by TTBK2 is necessary for cilia initiation.* J Cell Biol, 2019. **218**(10): p. 3489-
1078 3505.

1079 18. Graser, S., Y.D. Stierhof, S.B. Lavoie, O.S. Gassner, S. Lamla, M. Le Clech, *et al.*, *Cep164,*
1080 *a novel centriole appendage protein required for primary cilium formation.* J Cell Biol,
1081 2007. **179**(2): p. 321-30.
1082 19. Goetz, S.C., K.F. Liem, Jr., and K.V. Anderson, *The spinocerebellar ataxia-associated gene*
1083 *Tau tubulin kinase 2 controls the initiation of ciliogenesis.* Cell, 2012. **151**(4): p. 847-58.
1084 20. Schmidt, K.N., S. Kuhns, A. Neuner, B. Hub, H. Zentgraf, and G. Pereira, *Cep164 mediates*
1085 *vesicular docking to the mother centriole during early steps of ciliogenesis.* J Cell Biol,
1086 2012. **199**(7): p. 1083-101.
1087 21. Tanos, B.E., H.J. Yang, R. Soni, W.J. Wang, F.P. Macaluso, J.M. Asara, *et al.*, *Centriole*
1088 *distal appendages promote membrane docking, leading to cilia initiation.* Genes Dev, 2013.
1089 **27**(2): p. 163-8.
1090 22. Ye, X., H. Zeng, G. Ning, J.F. Reiter, and A. Liu, *C2cd3 is critical for centriolar distal*
1091 *appendage assembly and ciliary vesicle docking in mammals.* Proc Natl Acad Sci U S A,
1092 2014. **111**(6): p. 2164-9.
1093 23. Kurtulmus, B., C. Yuan, J. Schuy, A. Neuner, S. Hata, G. Kalamakis, *et al.*, *LRRC45*
1094 *contributes to early steps of axoneme extension.* J Cell Sci, 2018. **131**(18).
1095 24. Kanie, T., K.L. Abbott, N.A. Mooney, E.D. Plowey, J. Demeter, and P.K. Jackson, *The*
1096 *CEP19-RABL2 GTPase Complex Binds IFT-B to Initiate Intraflagellar Transport at the*
1097 *Ciliary Base.* Dev Cell, 2017. **42**(1): p. 22-36 e12.
1098 25. Nishijima, Y., Y. Hagiya, T. Kubo, R. Takei, Y. Katoh, and K. Nakayama, *RABL2 interacts*
1099 *with the intraflagellar transport-B complex and CEP19 and participates in ciliary assembly.*
1100 Mol Biol Cell, 2017. **28**(12): p. 1652-1666.
1101 26. Mojarad, B.A., G.D. Gupta, M. Hasegan, O. Goudiam, R. Basto, A.C. Gingras, *et al.*,
1102 *CEP19 cooperates with FOP and CEP350 to drive early steps in the ciliogenesis*
1103 *programme.* Open Biol, 2017. **7**(6).
1104 27. Hossain, D., Y. Javadi Esfehani, A. Das, and W.Y. Tsang, *Cep78 controls centrosome*
1105 *homeostasis by inhibiting EDD-DYRK2-DDB1 VprBP.* EMBO Rep, 2017. **18**(4): p. 632-
1106 644.
1107 28. Yoshida, S., K. Aoki, K. Fujiwara, T. Nakakura, A. Kawamura, K. Yamada, *et al.*, *The*
1108 *novel ciliogenesis regulator DYRK2 governs Hedgehog signaling during mouse*
1109 *embryogenesis.* Elife, 2020. **9**.
1110 29. Nikopoulos, K., P. Farinelli, B. Giangreco, C. Tsika, B. Royer-Bertrand, M.K. Mbefo, *et al.*,
1111 *Mutations in CEP78 Cause Cone-Rod Dystrophy and Hearing Loss Associated with*
1112 *Primary-Cilia Defects.* Am J Hum Genet, 2016. **99**(3): p. 770-776.
1113 30. Ascari, G., F. Peelman, P. Farinelli, T. Rosseel, N. Lambrechts, K.A. Wunderlich, *et al.*,
1114 *Functional characterization of the first missense variant in CEP78, a founder allele*
1115 *associated with cone-rod dystrophy, hearing loss, and reduced male fertility.* Hum Mutat,
1116 2020. **41**(5): p. 998-1011.
1117 31. Namburi, P., R. Ratnapriya, S. Khateb, C.H. Lazar, Y. Kinarty, A. Obolensky, *et al.*, *Bi-*
1118 *allelic Truncating Mutations in CEP78, Encoding Centrosomal Protein 78, Cause Cone-*
1119 *Rod Degeneration with Sensorineural Hearing Loss.* Am J Hum Genet, 2016. **99**(5): p.
1120 1222-1223.
1121 32. Fu, Q., M. Xu, X. Chen, X. Sheng, Z. Yuan, Y. Liu, *et al.*, *CEP78 is mutated in a distinct*
1122 *type of Usher syndrome.* J Med Genet, 2017. **54**(3): p. 190-195.
1123 33. de Castro-Miro, M., R. Tonda, P. Escudero-Ferruz, R. Andres, A. Mayor-Lorenzo, J. Castro,
1124 *et al.*, *Novel Candidate Genes and a Wide Spectrum of Structural and Point Mutations*
1125 *Responsible for Inherited Retinal Dystrophies Revealed by Exome Sequencing.* PLoS One,
1126 2016. **11**(12): p. e0168966.

1127 34. Azimzadeh, J., M.L. Wong, D.M. Downhour, A. Sanchez Alvarado, and W.F. Marshall,
1128 *Centrosome loss in the evolution of planarians.* Science, 2012. **335**(6067): p. 461-3.
1129 35. Brunk, K., M. Zhu, F. Barenz, A.S. Kratz, U. Haselmann-Weiss, C. Antony*, et al.*, *Cep78 is*
1130 *a new centriolar protein involved in Plk4-induced centriole overduplication.* J Cell Sci,
1131 2016. **129**(14): p. 2713-8.
1132 36. Knudsen, E.S. and J.Y. Wang, *Dual mechanisms for the inhibition of E2F binding to RB by*
1133 *cyclin-dependent kinase-mediated RB phosphorylation.* Mol Cell Biol, 1997. **17**(10): p.
1134 5771-5783.
1135 37. Paridaen, J.T., M. Wilsch-Brauninger, and W.B. Huttner, *Asymmetric inheritance of*
1136 *centrosome-associated primary cilium membrane directs ciliogenesis after cell division.*
1137 Cell, 2013. **155**(2): p. 333-44.
1138 38. Yan, X., R. Habedanck, and E.A. Nigg, *A complex of two centrosomal proteins, CAP350*
1139 *and FOP, cooperates with EB1 in microtubule anchoring.* Mol Biol Cell, 2006. **17**(2): p.
1140 634-644.
1141 39. Wang, L., M. Failler, W. Fu, and B.D. Dynlacht, *A distal centriolar protein network*
1142 *controls organelle maturation and asymmetry.* Nat Commun, 2018. **9**(1): p. 3938.
1143 40. Paintrand, M., M. Moudjou, H. Delacroix, and M. Bornens, *Centrosome organization and*
1144 *centriole architecture: their sensitivity to divalent cations.* J Struct Biol, 1992. **108**(2): p.
1145 107-128.
1146 41. Kim, J., J.E. Lee, S. Heynen-Genel, E. Suyama, K. Ono, K. Lee*, et al.*, *Functional genomic*
1147 *screen for modulators of ciliogenesis and cilium length.* Nature, 2010. **464**(7291): p. 1048-
1148 51.
1149 42. Shearer, R.F., K.M. Frikstad, J. McKenna, R.A. McCloy, N. Deng, A. Burgess*, et al.*, *The*
1150 *E3 ubiquitin ligase UBR5 regulates centriolar satellite stability and primary cilia.* Mol Biol
1151 Cell, 2018. **29**(13): p. 1542-1554.
1152 43. Tsang, W.Y. and B.D. Dynlacht, *CP110 and its network of partners coordinately regulate*
1153 *cilia assembly.* Cilia, 2013. **2**(1): p. 9.
1154 44. Yadav, S.P., N.K. Sharma, C. Liu, L. Dong, T. Li, and A. Swaroop, *Centrosomal protein*
1155 *CP110 controls maturation of the mother centriole during cilia biogenesis.* Development,
1156 2016. **143**(9): p. 1491-501.
1157 45. Walentek, P., I.K. Quigley, D.I. Sun, U.K. Sajjan, C. Kintner, and R.M. Harland, *Ciliary*
1158 *transcription factors and miRNAs precisely regulate Cp110 levels required for ciliary*
1159 *adhesions and ciliogenesis.* Elife, 2016. **5**.
1160 46. Loukil, A., K. Tormanen, and C. Sutterlin, *The daughter centriole controls ciliogenesis by*
1161 *regulating Neurl-4 localization at the centrosome.* J Cell Biol, 2017. **216**(5): p. 1287-1300.
1162 47. Nagai, T., S. Mukoyama, H. Kagiwada, N. Goshima, and K. Mizuno, *Cullin-3-KCTD10-*
1163 *mediated CEP97 degradation promotes primary cilium formation.* J Cell Sci, 2018. **131**(24).
1164 48. Wheway, G., M. Schmidts, D.A. Mans, K. Szymanska, T.T. Nguyen, H. Racher*, et al.*, *An*
1165 *siRNA-based functional genomics screen for the identification of regulators of ciliogenesis*
1166 *and ciliopathy genes.* Nat Cell Biol, 2015. **17**(8): p. 1074-1087.
1167 49. Nakagawa, T., K. Mondal, and P.C. Swanson, *VprBP (DCAF1): a promiscuous substrate*
1168 *recognition subunit that incorporates into both RING-family CRL4 and HECT-family*
1169 *EDD/UBR5 E3 ubiquitin ligases.* BMC Mol Biol, 2013. **14**: p. 22.
1170 50. Patzke, S., S. Redick, A. Warsame, C.A. Murga-Zamalloa, H. Khanna, S. Doxsey*, et al.*,
1171 *CSPP is a ciliary protein interacting with Nephrocystin 8 and required for cilia formation.*
1172 Molecular biology of the cell, 2010. **21**(15): p. 2555-67.

1173 51. Frikstad, K.M., E. Molinari, M. Thoresen, S.A. Ramsbottom, F. Hughes, S.J.F. Letteboer, *et*
1174 *al.*, *A CEP104-CSPP1 Complex Is Required for Formation of Primary Cilia Competent in*
1175 *Hedgehog Signaling.* Cell Rep, 2019. **28**(7): p. 1907-1922 e6.
1176 52. Jiang, K., G. Toedt, S. Montenegro Gouveia, N.E. Davey, S. Hua, B. van der Vaart, *et al.*, *A*
1177 *Proteome-wide screen for mammalian SxIP motif-containing microtubule plus-end tracking*
1178 *proteins.* Curr Biol, 2012. **22**(19): p. 1800-7.
1179 53. Satish Tammana, T.V., D. Tammana, D.R. Diener, and J. Rosenbaum, *Centrosomal protein*
1180 *CEP104 (Chlamydomonas FAP256) moves to the ciliary tip during ciliary assembly.* J Cell
1181 Sci, 2013. **126**(Pt 21): p. 5018-29.
1182 54. Eguether, T., M.A. Ermolaeva, Y. Zhao, M.C. Bonnet, A. Jain, M. Pasparakis, *et al.*, *The*
1183 *deubiquitinating enzyme CYLD controls apical docking of basal bodies in ciliated epithelial*
1184 *cells.* Nat Commun, 2014. **5**: p. 4585.
1185 55. Wang, L., K. Lee, R. Malonis, I. Sanchez, and B.D. Dynlacht, *Tethering of an E3 ligase by*
1186 *PCM1 regulates the abundance of centrosomal KIAA0586/Talpid3 and promotes*
1187 *ciliogenesis.* Elife, 2016. **5**.
1188 56. Douanne, T., G. Andre-Gregoire, A. Thys, K. Trillet, J. Gavard, and N. Bidere, *CYLD*
1189 *Regulates Centriolar Satellites Proteostasis by Counteracting the E3 Ligase MIB1.* Cell
1190 Rep, 2019. **27**(6): p. 1657-1665 e4.
1191 57. Yi, C., Z. Shen, A. Stemmer-Rachamimov, N. Dawany, S. Troutman, L.C. Showe, *et al.*,
1192 *The p130 isoform of angiomotin is required for Yap-mediated hepatic epithelial cell*
1193 *proliferation and tumorigenesis.* Sci Signal, 2013. **6**(291): p. ra77.
1194 58. Hoppeler-Lebel, A., C. Celati, G. Bellett, M.M. Mogensen, L. Klein-Hitpass, M. Bornens, *et*
1195 *al.*, *Centrosomal CAP350 protein stabilises microtubules associated with the Golgi*
1196 *complex.* J Cell Sci, 2007. **120**(Pt 18): p. 3299-308.
1197 59. Belzile, J.P., G. Duisit, N. Rougeau, J. Mercier, A. Finzi, and E.A. Cohen, *HIV-1 Vpr-*
1198 *mediated G2 arrest involves the DDB1-CUL4AVPRBP E3 ubiquitin ligase.* PLoS Pathog,
1199 2007. **3**(7): p. e85.
1200 60. Cox, J. and M. Mann, *MaxQuant enables high peptide identification rates, individualized*
1201 *p.p.b.-range mass accuracies and proteome-wide protein quantification.* Nat Biotechnol,
1202 2008. **26**(12): p. 1367-72.
1203 61. Schou, K.B., J.B. Mogensen, A. Aleliunaite, S.K. Morthorst, I.R. Veland, S.T. Christensen,
1204 *et al.*, *Kinesin-3 motor protein KIF13B localizes to centrosomes and primary cilia and*
1205 *regulates ciliary length and signaling.* Cilia, 2014. **4**(Suppl 1): p. O3.
1206 62. Verdier, P., S.K. Morthorst, and L.B. Pedersen, *Targeting of ASH Domain-Containing*
1207 *Proteins to the Centrosome.* Methods Mol Biol, 2016. **1454**: p. 15-33.
1208 63. Langmead, B. and S.L. Salzberg, *Fast gapped-read alignment with Bowtie 2.* Nat Methods,
1209 2012. **9**(4): p. 357-9.
1210 64. Kim, D., G. Pertea, C. Trapnell, H. Pimentel, R. Kelley, and S.L. Salzberg, *TopHat2:*
1211 *accurate alignment of transcriptomes in the presence of insertions, deletions and gene*
1212 *fusions.* Genome Biol, 2013. **14**(4): p. R36.
1213 65. Anders, S., P.T. Pyl, and W. Huber, *HTSeq--a Python framework to work with high-*
1214 *throughput sequencing data.* Bioinformatics, 2015. **31**(2): p. 166-9.
1215 66. Trapnell, C., B.A. Williams, G. Pertea, A. Mortazavi, G. Kwan, M.J. van Baren, *et al.*,
1216 *Transcript assembly and quantification by RNA-Seq reveals unannotated transcripts and*
1217 *isoform switching during cell differentiation.* Nat Biotechnol, 2010. **28**(5): p. 511-5.
1218 67. Robinson, M.D., D.J. McCarthy, and G.K. Smyth, *edgeR: a Bioconductor package for*
1219 *differential expression analysis of digital gene expression data.* Bioinformatics, 2010. **26**(1):
1220 p. 139-40.

1221 68. Love, M.I., W. Huber, and S. Anders, *Moderated estimation of fold change and dispersion*
1222 *for RNA-seq data with DESeq2.* Genome Biol, 2014. **15**(12): p. 550.
1223

1224 **Appendix**

1225 **Key Resources Table**

Reagent type (species) or resource	**Designation**	**Source or reference**	**Identifier**	**Additional information**
Cell line (*H. sapiens*)	hTERT-RPE1	ATCC	Cat# CRL-4000	Derived from human retinal pigment epithelium
Cell line (*H. sapiens*)	Puromycin-sensitive hTERT-RPE1	Francesc Garcia-Gonzalo, Autonomous University of Madrid, Madrid, Spain	N/A	
Cell line (*H. sapiens*)	hTERT-RPE1 *CEP78* KO	[30]	Clone #73	
Cell line (*H. sapiens*)	hTERT-RPE1 *CEP78* KO	This study	Clone #44	Generated as described in [30]; contains px459-Cas9 plasmid inserted in exon 1
Cell line (*H. sapiens*)	hTERT-RPE1 *CEP78* KO	This study	Clone #52	Generated as described in [30]; contains homozygous frameshift mutation in exon 1 of *CEP78* (single nucleotide insertion in codon 10; GAC>GAAC)

Cell line (*H. sapiens*)	hTERT-RPE1 *CEP78* KO	This study	Clone #2	Generated as described in [30]; homozygous frameshift mutation in exon 1 of *CEP78* (single nucleotide insertion in codon 10; GAC>GAAC)
Cell line (*H. sapiens*)	hTERT-RPE1 *CEP78* KO/mNG-CEP78	This study	N/A	Parental line is *CEP78* KO clone #73
Cell line (*H. sapiens*)	hTERT-RPE1 *CEP78* KO/mNG-CEP78^{L150S}	This study	N/A	Parental line is *CEP78* KO clone #73
Cell line (*H. sapiens*)	hTERT-RPE1 WT/mNG-CEP78	This study	N/A	Parental line is puromycin-sensitive hTERT-RPE listed above
Cell line (*H. sapiens*)	hTERT-RPE1-BFP-Cas9/pMCB306 (pool)	[24]	N/A	Control cell line for *CEP350* and *FOP* KO lines
Cell line (*H. sapiens*)	hTERT-RPE1-BFP-Cas9/ *CEP350* KO (pool)	[24]	N/A	
Cell line (*H. sapiens*)	hTERT-RPE1-BFP-Cas9/*FOP* KO (pool)	[24]	N/A	
Cell line (*H. sapiens*)	293T	ATCC	Cat# CRL-3216	Derived from human embryonic kidney
Cell line (*H. sapiens*)	Control skin fibroblasts	[29]	N/A	Primary cells
Cell line (*H. sapiens*)	Compound heterozygous skin fibroblasts with two *CEP78* mutations: c.449T>C; p.Leu150Ser and c.1462-1G>T	[30]	F3: II:1	Primary cells; these cells do not express detectable levels of CEP78 [30]

Cell line (*H. sapiens*)	Compound heterozygous skin fibroblasts with two *CEP78* mutations: c.633delC; p.Trp212Glyfs*18 and c.499+5G>A; IVS + 5G>A	[29]	2702r34, individual II-3	Primary cells; these cells do not express detectable levels of CEP78 [29]
Cell line (*H. sapiens*)	Homozygous substitution in the first invariant base of intron 3 splice donor site in *CEP78*: c.499+1G>T (IVS3+1G>T)	[29]	KN10, individual II-1	Primary cells; these cells express almost undetectable levels of CEP78 [29]
Strain, strain background (*E. coli*)	DH10B	Lab stock	N/A	
Antibody	Anti-Acetylated-tubulin (mouse monoclonal)	Sigma-Aldrich	Cat# T7451	IFM (1:2000)
Antibody	Anti-α-tubulin (mouse monoclonal)	Sigma-Aldrich	Cat# T5168	WB (1:10000)
Antibody	Anti-ARL13B (rabbit polyclonal)	Proteintech	Cat# 17711-1-AP	IFM (1:500)
Antibody	Anti-CEP78 (rabbit polyclonal)	Bethyl Laboratories	Cat# A301-799A-M	IFM (1:200) WB (1:500)
Antibody	Anti-CEP164 (rabbit polyclonal)	Sigma-Aldrich	Cat# HPA037606	IFM (1:500)
Antibody	Anti-CEP350 (mouse monoclonal)	Abcam	Cat# Ab219831 (CL3423)	IFM (1:500)
Antibody	Anti-CEP350 (rabbit polyclonal)	Novus Biologicals	Cat# NB100-59811	IFM (1:200)
Antibody	Anti-CP110 (rabbit polyclonal)	Proteintech	Cat# 12780-1-AP	IFM (1:200) WB (1:1500)

Antibody	Anti-DCTN1/P-150 (mouse monoclonal)	BD Biosciences	Cat# 610474	IFM (1:500)
Antibody	Anti-EDD1 (rabbit polyclonal)	Bethyl Laboratories	Cat# A300-573A-M	IFM (1:100)
Antibody	Anti-FLAG (mouse monoclonal)	Sigma-Aldrich	Cat# F1804	IFM (1:500) WB (1:1000)
Antibody	Anti-FLAG (rabbit polyclonal)	Sigma-Aldrich	Cat# F7425	WB (1:1000)
Antibody	Anti-FGFR1OP/FOP (mouse monoclonal)	Novus Biologicals	Cat# H00011116-M01	WB (1:500)
Antibody	Anti-GAPDH (rabbit polyclonal)	Cell Signaling Technology	Cat# 2118	WB (1:1000)
Antibody	Anti-GFP (rabbit polyclonal)	Sigma-Aldrich	Cat# SAB4301138	WB (1:500)
Antib0dy	Anti-GFP (rabbit polyclonal)	Santa Cruz Biotechnologies, Inc.	Cat# sc-8834	WB (1:500)
Antibody	Anti-Myc (mouse monoclonal, 9B11)	Cell Signaling Technology	Cat# 2276S	WB (1:1000)
Antibody	Anti-phospho Rb (S807/811) (mouse monoclonal)	Cell Signaling Technology	Cat# 9308	WB (1:500)
Antibody	Anti-VPRBP (rabbit polyclonal)	Bethyl Laboratories	Cat# A301-877A-M	WB (1:200)
Antibody	Polyclonal Goat Anti-Mouse Immunoglobulins /Horseradish Peroxidase conjugated	Dako	Cat# P0447	WB (1:10000)
Antibody	Polyclonal Swine Anti-Rabbit Immunoglobulins /Horseradish Peroxidase conjugated	Dako	Cat# P0399	WB (1:10000)

Antibody	Donkey anti-Mouse IgG (H+L) Highly Cross-Adsorbed Secondary Antibody/Alexa Fluor 488-conjugated	Thermo Fisher Scientific	Cat# A21202	IFM (1:500)
Antibody	Donkey anti-Mouse IgG (H+L) Highly Cross-Adsorbed Secondary Antibody/Alexa Fluor 568-conjugated	Thermo Fisher Scientific	Cat # A10037	IFM (1:500)
Antibody	Donkey anti-Rabbit IgG (H+L) Highly Cross-Adsorbed Secondary Antibody/Alexa Fluor 488-conjugated	Thermo Fisher Scientific	Cat #A21206	IFM (1:500)
Antibody	Donkey anti-Rabbit IgG (H+L) Highly Cross-Adsorbed Secondary Antibody/Alexa Fluor 568-conjugated	Thermo Fisher Scientific	Cat# A10042	IFM (1:500)
Antibody	AffiniPure Donkey Anti-Mouse IgG (H+L)/Alexa Fluor® 647-conjugated	Jackson ImmunoResearch	Cat# 715-605-150	IFM (1:1000)
Antibody	Donkey Anti-Rabbit IgG H&L Secondary Antibodies/ Dylight® 550-conjugated	Abcam	Cat# ab96892	IFM (1:1000)
Enzyme	USER® Enzyme	New England BioLabs	Cat# M5505L	
Enzyme	Phusion® High-Fidelity DNA polymerase	New England BioLabs	Cat# M0530L	

Recombinant DNA reagent	*H. sapiens* Angiomotin p80 (Ap80)/pCMV-FLAG	[57]	N/A	
Recombinant DNA reagent	*H. sapiens* CEP78 aa 2-217/pEGFP-C1	This study	CEP78 N-terminus (N)	PCR-amplified using primers h.CEP78.4f.kpn1 and hsEGFP-CEP78_Rv (651)
Recombinant DNA reagent	*H. sapiens* CEP78 aa 203-403/pEGFP-C1	This study	CEP78 Middle (M)	PCR-amplified using primers hsEGFP-CEP78_Fwd (607) and hsEGFP-CEP78_Rv (1209)
Recombinant DNA reagent	*H. sapiens* CEP78 aa 2-403/pEGFP-C1	This study	CEP78 N-terminus plus Middle (NM)	PCR-amplified using primers h.CEP78.4f.kpn1 and hsEGFP-CEP78_Rv (1209)
Recombinant DNA reagent	*H. sapiens* CEP78 aa 395-722/pEGFP-C1	This study	CEP78 C-terminus (C)	PCR-amplified using primers hsEGFP-CEP78_Fwd (1186) and hCEP78.rv_stop. bamh1
Recombinant DNA reagent	*H. sapiens* CEP78/pEGFP-C1	This study	N/A	PCR-amplified using primers h.CEP78.4f.kpn1 and hCEP78.rv_stop. bamh1
Recombinant DNA reagent	*H. sapiens* CEP78/p3xFLAG-CMV/DEST	This study	p3xFLAG-CEP78	
Recombinant DNA reagent	*H. sapiens* CEP78^{L150S}/p p3xFLAG-CMV/DEST	This study	p3xFLAG-CEP78^{L150S}	
Recombinant DNA reagent	Plasmid pEGFP-C1 (empty vector)	TaKaRa Bio	Cat# 6084-1	

Recombinant DNA reagent	Gateway® pDONR™201	Invitrogen/Thermo Fisher Scientific	Cat# 11798-014	
Recombinant DNA reagent	p3xFLAG-CMV-10	Sigma-Aldrich	Cat# E7658	Cloning produces in-frame 3xFLAG tag in the N-terminus
Recombinant DNA reagent	p3xFLAG-CMV/DEST	Gift from Ronald Roepman lab, Radboud University Medical Center, Nijmegen, NL	pDEST306	p3xFLAG-CMV-10 with Gateway Rf-B cassette inserted into the blunted HindIII/BamHI site
Recombinant DNA reagent	*H. sapiens* CEP350 aa 1-983/pCS2^{+} with a 6×myc tag	[54, 58]	CAP N	
Recombinant DNA reagent	*H. sapiens* CEP350 aa 2990-3117/pCS2^{+} with a 6×myc tag	[54, 58]	CAP C	
Recombinant DNA reagent	*H. sapiens* VPRBP/pCMV-Myc	[59]	Myc-VPRBP	Cloned in Sal1 and Not1 sites
Sequence-based reagent	*H. sapiens CEP78* ORF/ GeneCopoiea pShuttle™Gateway® PLUS ORF	GeneCopoiea	NCBI reference Sequence NM_001098802.3	
Sequence-based reagent	*H. sapiens CEP78* PCR primer	Sigma-Aldrich	attB forward	5'-GGGACAAGTTGTACAAAAAACAGGCTTCATCGACTCCGTGAAGCTGC-3'
Sequence-based reagent	*H. sapiens CEP78* PCR primer	Sigma-Aldrich	attB reverse	5-GGGGACCACTTTGTACAAGAAAGCTGGGTTTCAGGAATGCAGGTCCTTTCCAG-3'

Sequence-based reagent	*H. sapiens CEP78* PCR primer	Sigma-Aldrich	CEP78 mut_F	5'-AGAGACAGGTGCACCGAAGAAGCCGATTTATTCAATC-3'
Sequence-based reagent	*H. sapiens CEP78* PCR primer	Sigma-Aldrich	CEP78 mut_R	5'-GATTGAATAAATCGGCTTCTTCGGTGCACCTGTCTCT-3'
Sequence-based reagent	*H. sapiens CEP78* PCR primer	Eurofins Genomics	hCEP78.4f.kpn1	5'-AAGGTACCATCGACTCCGTGAAGCTGCG-3'
Sequence-based reagent	*H. sapiens CEP78* PCR primer	Eurofins Genomics	hsEGFP-CEP78_Rv (651)	5'-AAGGATCCTTAGCGAAGACTCTCAGCCCAG-3'
Sequence-based reagent	*H. sapiens CEP78* PCR primer	Eurofins Genomics	hsEGFP-CEP78_Fwd (607)	5'- GGGGTACCCAGACCATGAGAAGGCATGA -3'
Sequence-based reagent	*H. sapiens CEP78* PCR primer	Eurofins Genomics	hsEGFP-CEP78_Rv (1209)	5'-GGGGATCCTTAACCCCTGTGTCTTTTTGCAC-3'
Sequence-based reagent	*H. sapiens CEP78* PCR primer	Eurofins Genomics	hsEGFP-CEP78_Fwd (1186)	5'-GGGGTACCGCAGAACGTGCAAAAAGACA-3'
Sequence-based reagent	*H. sapiens CEP78* PCR primer	Eurofins Genomics	hCEP78.rv_stop. bamh1	5'-GAGGATCCACAGGAATGCAGGTCCTTTC-3'
Sequence-based reagent	Control siRNA	Eurofins Genomics	N/A	5'-UAAUGUAUUGGAAGGCA-3'

Sequence-based reagent	*H. sapiens CP110* siRNA	Eurofins Genomics /[5]	N/A	5'-GCAAAACCAGAAUACGAGATT-3'
Chemical compound, drug	DAPI (4′, 6-diamidino-2-phenylindole)	Thermo Fisher Scientific	Cat# D1306	Stored at -20ºC as stock solution of 20 µg/ml in H_2O
Chemical compound drug	FuGENE®6	Promega	Cat# E2692	
Chemical compound, drug	DharmaFECT™ Duo Transfection reagent	Dharmacon™	Cat# T-2010-03	
Software, algorithm	cellSens Dimension	Olympus	Version 1.18	
Software, algorithm	Zen Black 2012	Zeiss	Version 2012	
Software, algorithm	Adobe Photoshop®	Adobe	Version 21.0.1	
Software, algorithm	Adobe Illustrator®	Adobe	Version 24.2.1	
Software, algorithm	ImageJ	NIH	Mac OS X or Windows	
Software, algorithm	GraphPad Prism 6.0	GraphPad Software Inc.	Mac OS X or Windows	
Software, algorithm	MaxQuant	[60]	Version 1.6.1.0	
Other	Anti-FLAG® M2 Affinity Gel	Sigma-Aldrich	Cat# A2220	
Other	Anti-c-Myc Agarose Affinity Gel antibody produced in rabbit	Sigma-Aldrich	Cat# A7470-1 ml	
Other	GFP-Trap® Agarose	ChromoTek GmbH	Cat# gta-20	
Other	QuickChange Lightning Site-Directed Mutagenesis Kit	Agilent	Cat# 210518	
Other	Direct-zol RNA Miniprep Kit	Zymo Research	Cat# R2051	
Other	Agilent RNA Nano 6000 Assay Kit	Agilent	Cat# 5067-1511	

Other	NEBNext® Ultra™ RNA Library Prep Kit for Illumina®	New England BioLabs	Cat# E7530L	
Other	Invitrogen™ Qubit® RNA Assay Kit	Thermo Fisher Scientific	Cat# 32852	
Other	AMPure XP system	Beckman Coulter Life Sciences	Cat# A63881	

1226

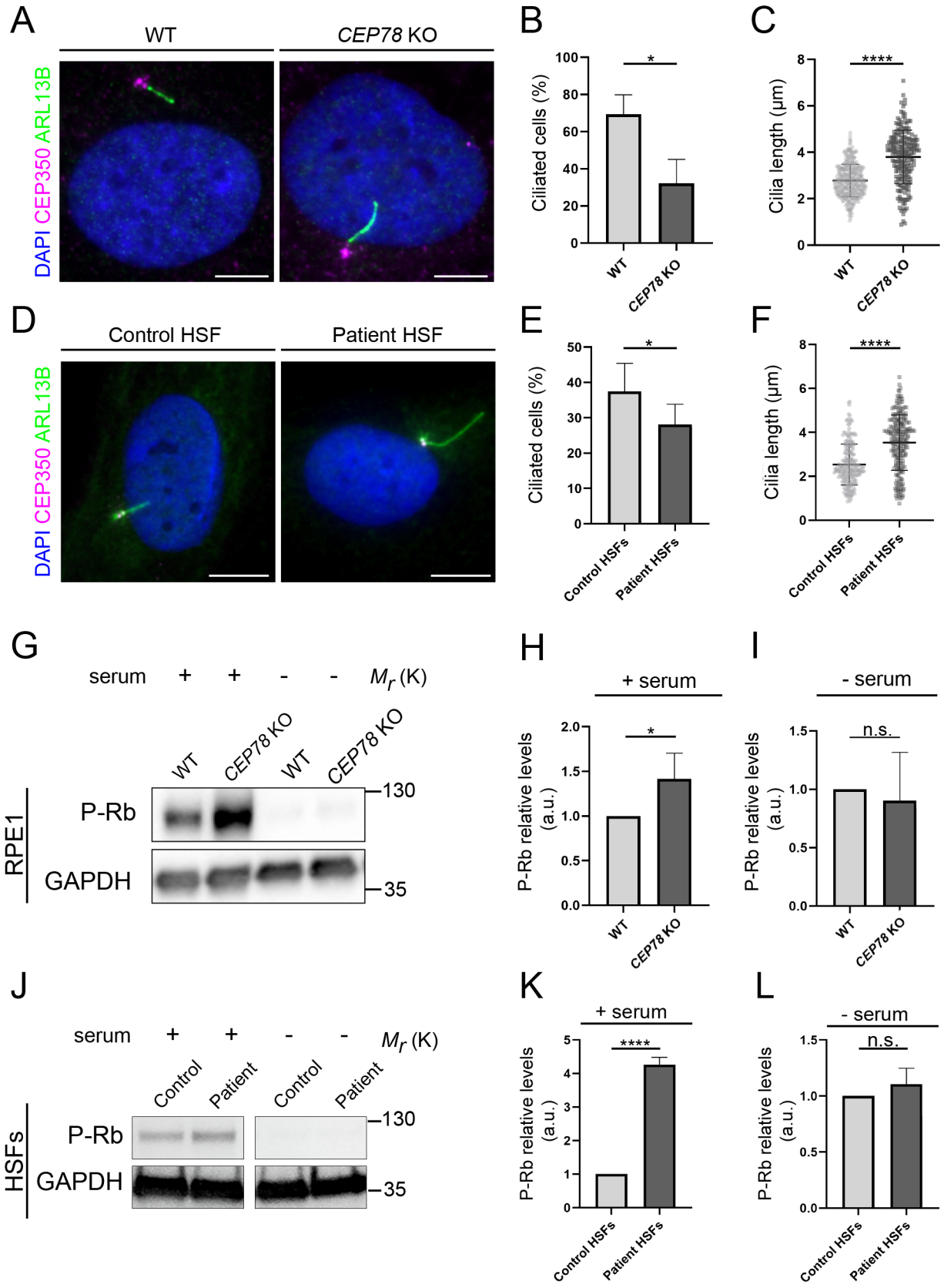
A
WT
CEP78 KO
DAPI CEP350 ARL13B
B
Ciliated cells (%)
*
WT
CEP78 KO
C
Cilia length (µm)
****
WT
CEP78 KO
D
Control HSF
Patient HSF
DAPI CEP350 ARL13B
E
Ciliated cells (%)
*
Control HSFs
Patient HSFs
F
Cilia length (µm)
****
Control HSFs
Patient HSFs
G
serum + + - - M_r (K)
WT
CEP78 KO
WT
CEP78 KO
RPE1
P-Rb
GAPDH
130
35
H
+ serum
P-Rb relative levels (a.u.)
*
WT
CEP78 KO
I
- serum
P-Rb relative levels (a.u.)
n.s.
WT
CEP78 KO
J
serum + + - - M_r (K)
Control
Patient
Control
Patient
HSFs
P-Rb
GAPDH
130
35
K
+ serum
P-Rb relative levels (a.u.)
****
Control HSFs
Patient HSFs
L
- serum
P-Rb relative levels (a.u.)
n.s.
Control HSFs
Patient HSFs

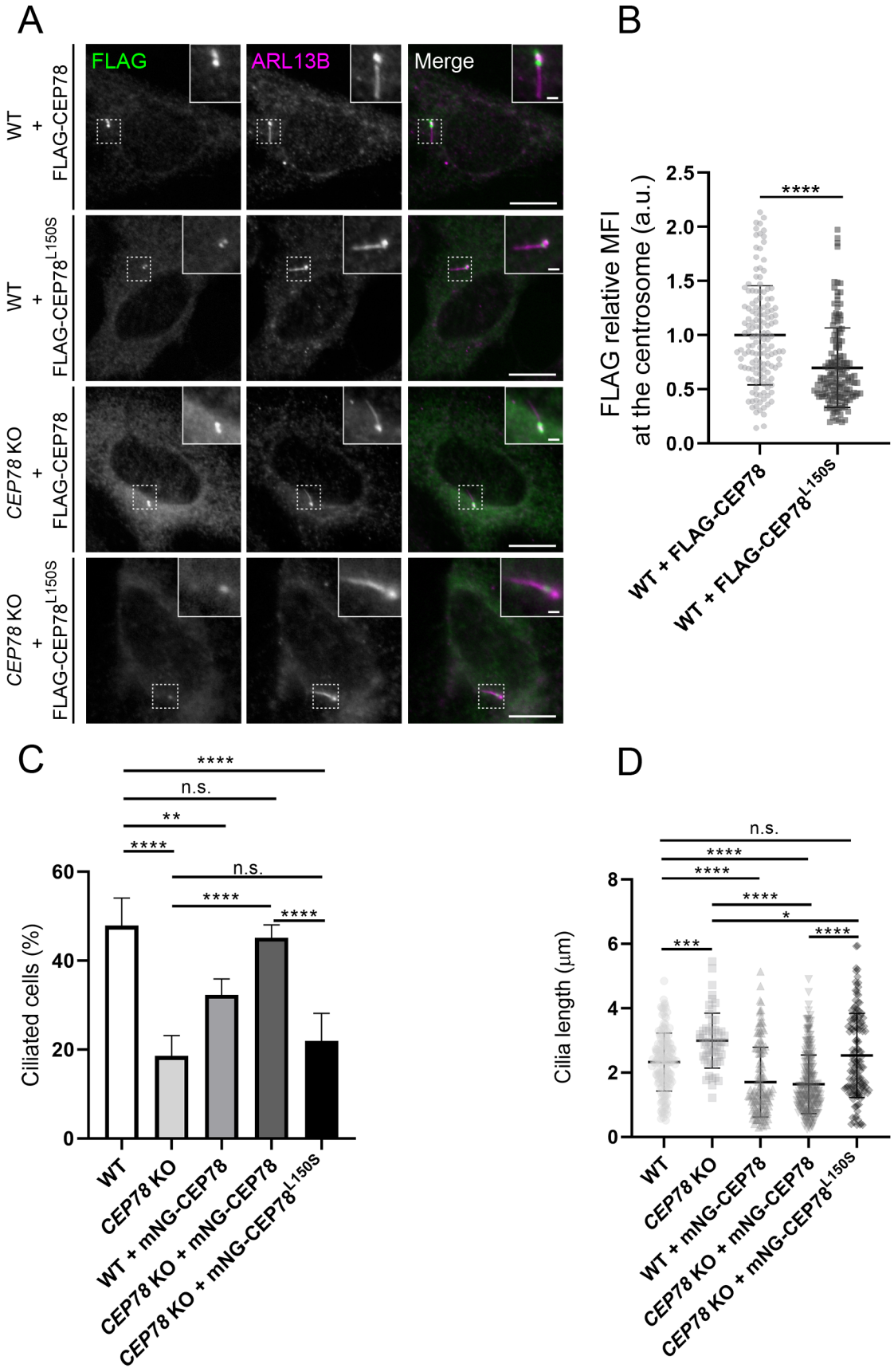
A
FLAG
ARL13B
Merge
WT + FLAG-CEP78
WT + FLAG-CEP78L150S
CEP78 KO + FLAG-CEP78
CEP78 KO + FLAG-CEP78L150S
B
FLAG relative MFI at the centrosome (a.u.)
2.5
2.0
1.5
1.0
0.5
0.0
****
WT + FLAG-CEP78
WT + FLAG-CEP78L150S
C
Ciliated cells (%)
60
40
20
0
****
n.s.
**
****
n.s.
****
****
WT
CEP78 KO
WT + mNG-CEP78
CEP78 KO + mNG-CEP78
CEP78 KO + mNG-CEP78L150S
D
Cilia length (µm)
8
6
4
2
0
n.s.
****
****
****
*
***
****
WT
CEP78 KO
WT + mNG-CEP78
CEP78 KO + mNG-CEP78
CEP78 KO + mNG-CEP78L150S

A

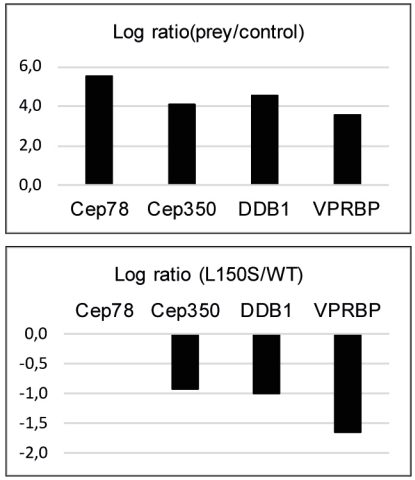
Log ratio(prey/control)
6,0
4,0
2,0
0,0
Cep78
Cep350
DDB1
VPRBP
Log ratio (L150S/WT)
Cep78
Cep350
DDB1
VPRBP
0,0
-0,5
-1,0
-1,5
-2,0

B

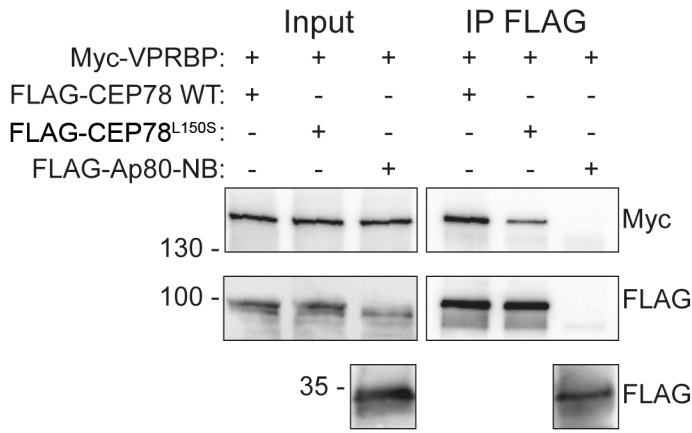
Input
IP FLAG
Myc-VPRBP: + + + + + +
FLAG-CEP78 WT: + - - + - -
FLAG-CEP78L150S: - + - - + -
FLAG-Ap80-NB: - - + - - +
130 -
100 -
35 -
Myc
FLAG
FLAG

C

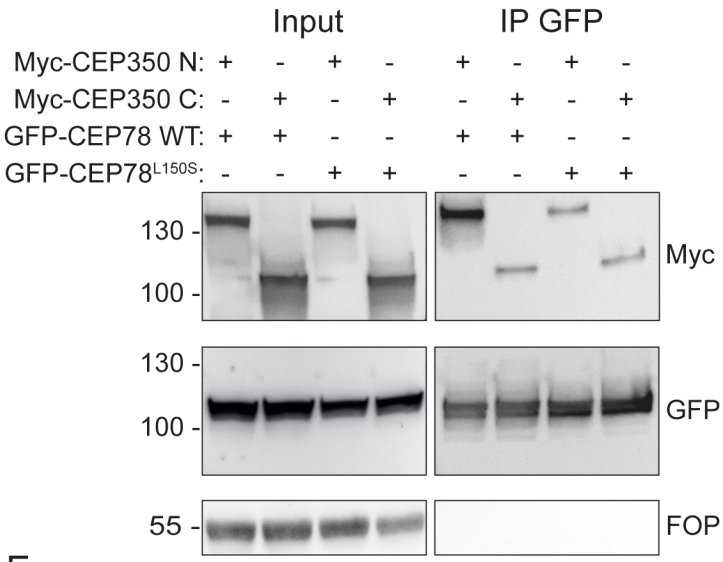
Input
IP GFP
Myc-CEP350 N: + - + - + - + -
Myc-CEP350 C: - + - + - + - +
GFP-CEP78 WT: + + - - + + - -
GFP-CEP78L150S: - - + + - - + +
130 -
100 -
130 -
100 -
55 -
Myc
GFP
FOP

D

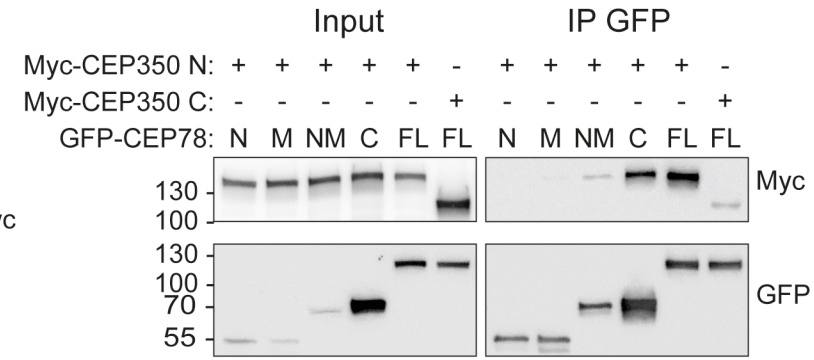
Input
IP GFP
Myc-CEP350 N: + + + + + - + + + + + -
Myc-CEP350 C: - - - - - + - - - - - +
GFP-CEP78: N M NM C FL FL N M NM C FL FL
130 -
100 -
130 -
100 -
70 -
55 -
Myc
GFP

E

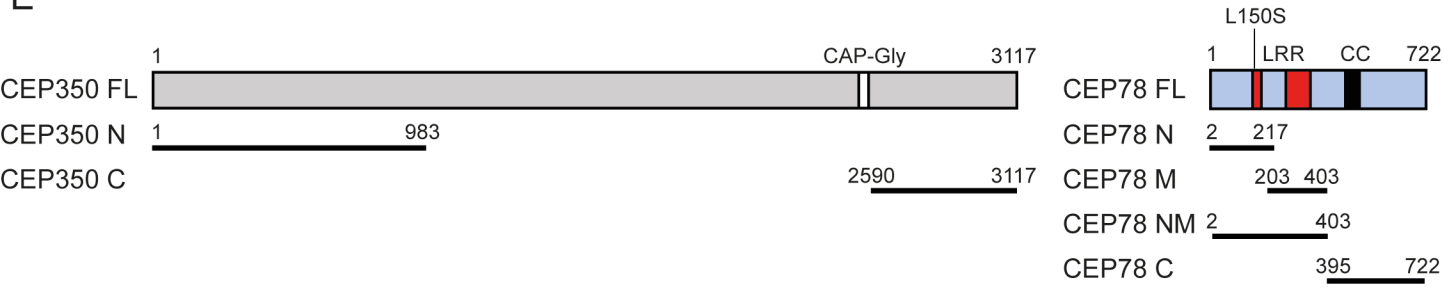
CEP350 FL
1
CAP-Gly
3117
CEP350 N
1
983
CEP350 C
2590
3117
L150S
1
LRR
CC
722
CEP78 FL
CEP78 N
2
217
CEP78 M
203
403
CEP78 NM
2
403
CEP78 C
395
722

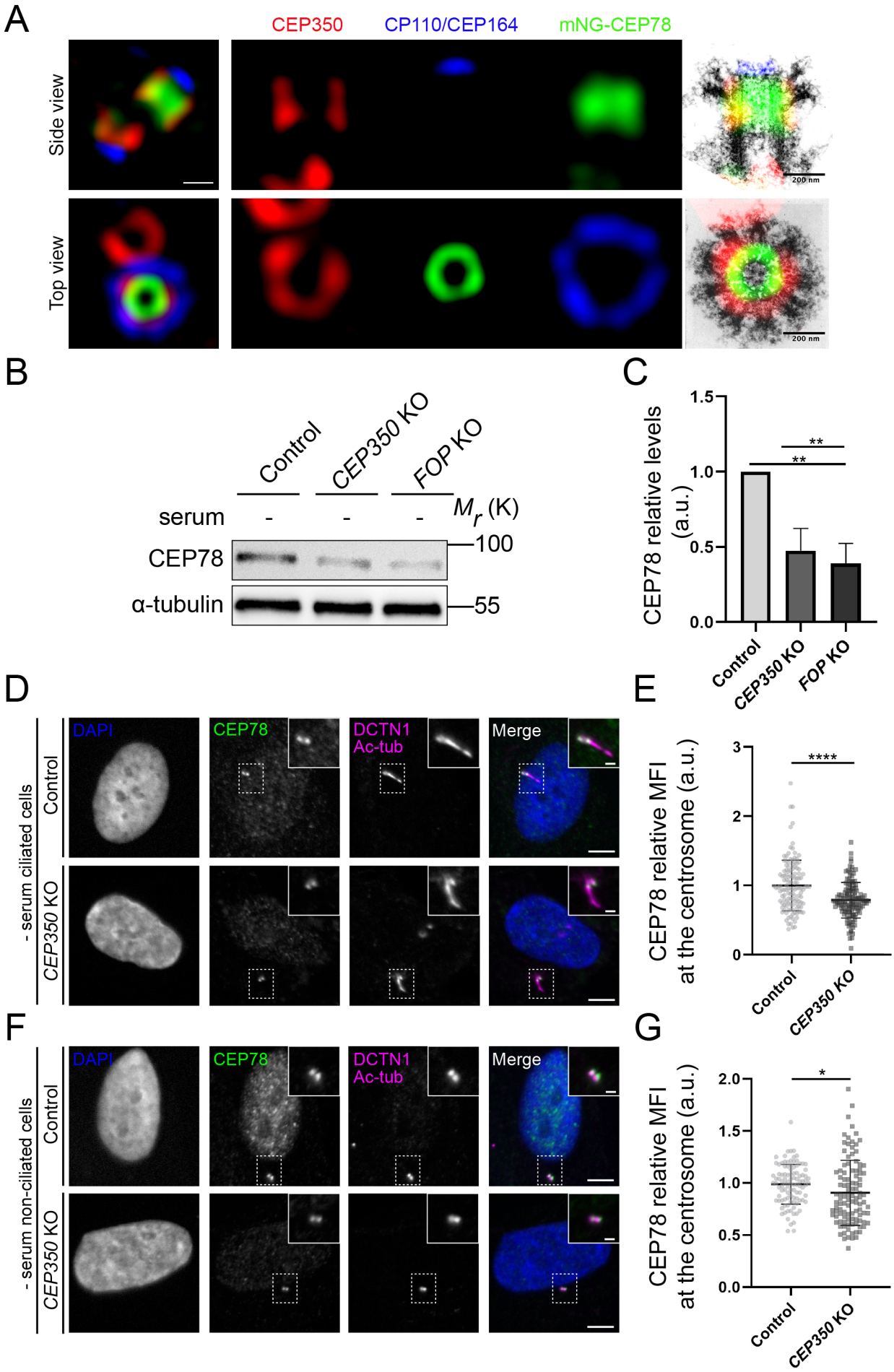
A
CEP350
CP110/CEP164
mNG-CEP78
Side view
Top view
200 nm
200 nm
B
Control
CEP350 KO
FOP KO
serum
-
-
-
M_r (K)
CEP78
100
α-tubulin
55
C
CEP78 relative levels (a.u.)
1.5
1.0
0.5
0.0
**
**
Control
CEP350 KO
FOP KO
D
- serum ciliated cells
Control
CEP350 KO
DAPI
CEP78
DCTN1
Ac-tub
Merge
E
CEP78 relative MFI at the centrosome (a.u.)
3
2
1
0
****
Control
CEP350 KO
F
- serum non-ciliated cells
Control
CEP350 KO
DAPI
CEP78
DCTN1
Ac-tub
Merge
G
CEP78 relative MFI at the centrosome (a.u.)
2.0
1.5
1.0
0.5
0.0
*
Control
CEP350 KO

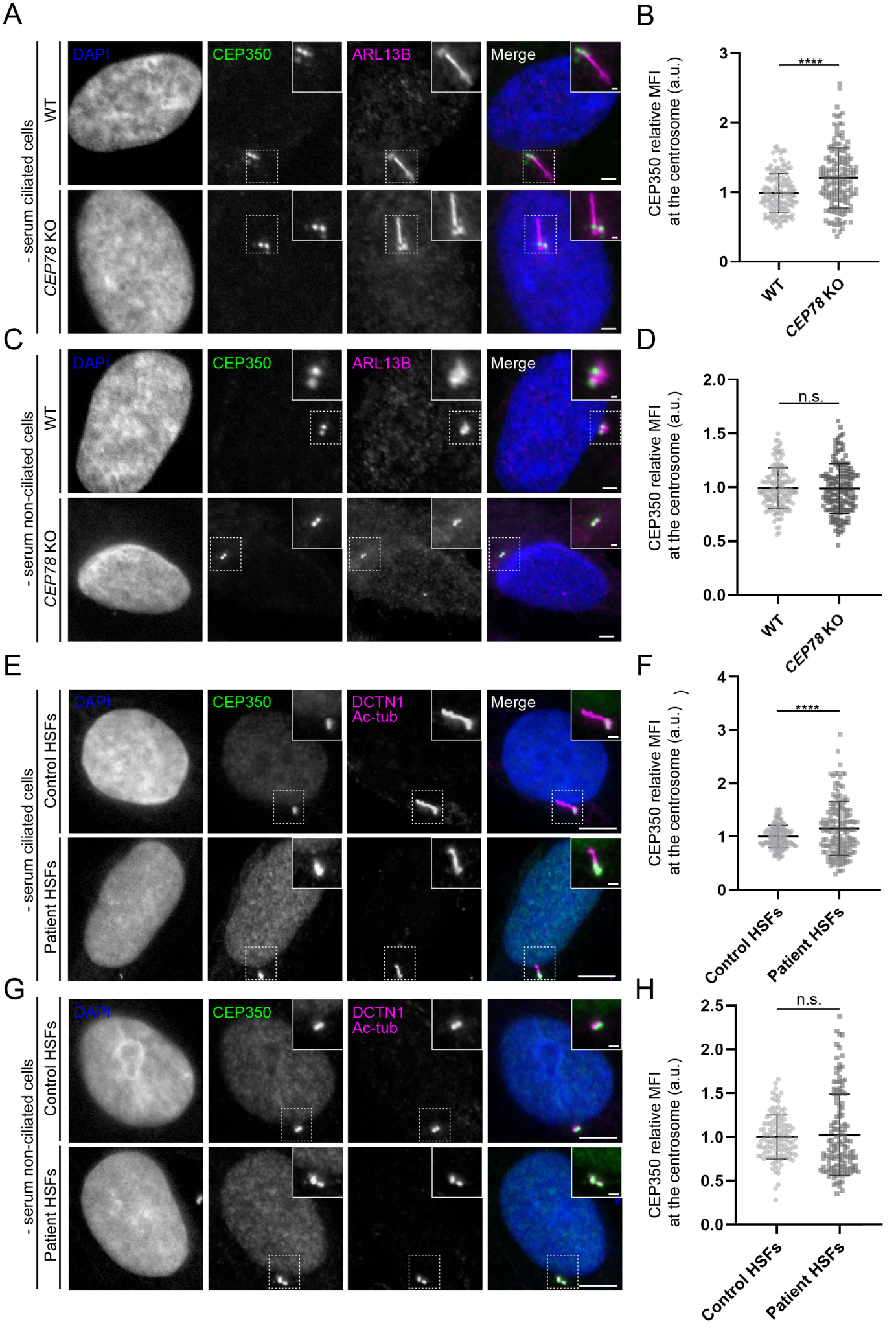
A
- serum ciliated cells
WT
CEP78 KO
DAPI
CEP350
ARL13B
Merge
B
CEP350 relative MFI at the centrosome (a.u.)
****
WT
CEP78 KO
C
- serum non-ciliated cells
D
n.s.
E
Control HSFs
Patient HSFs
DCTN1
Ac-tub
F
G
H

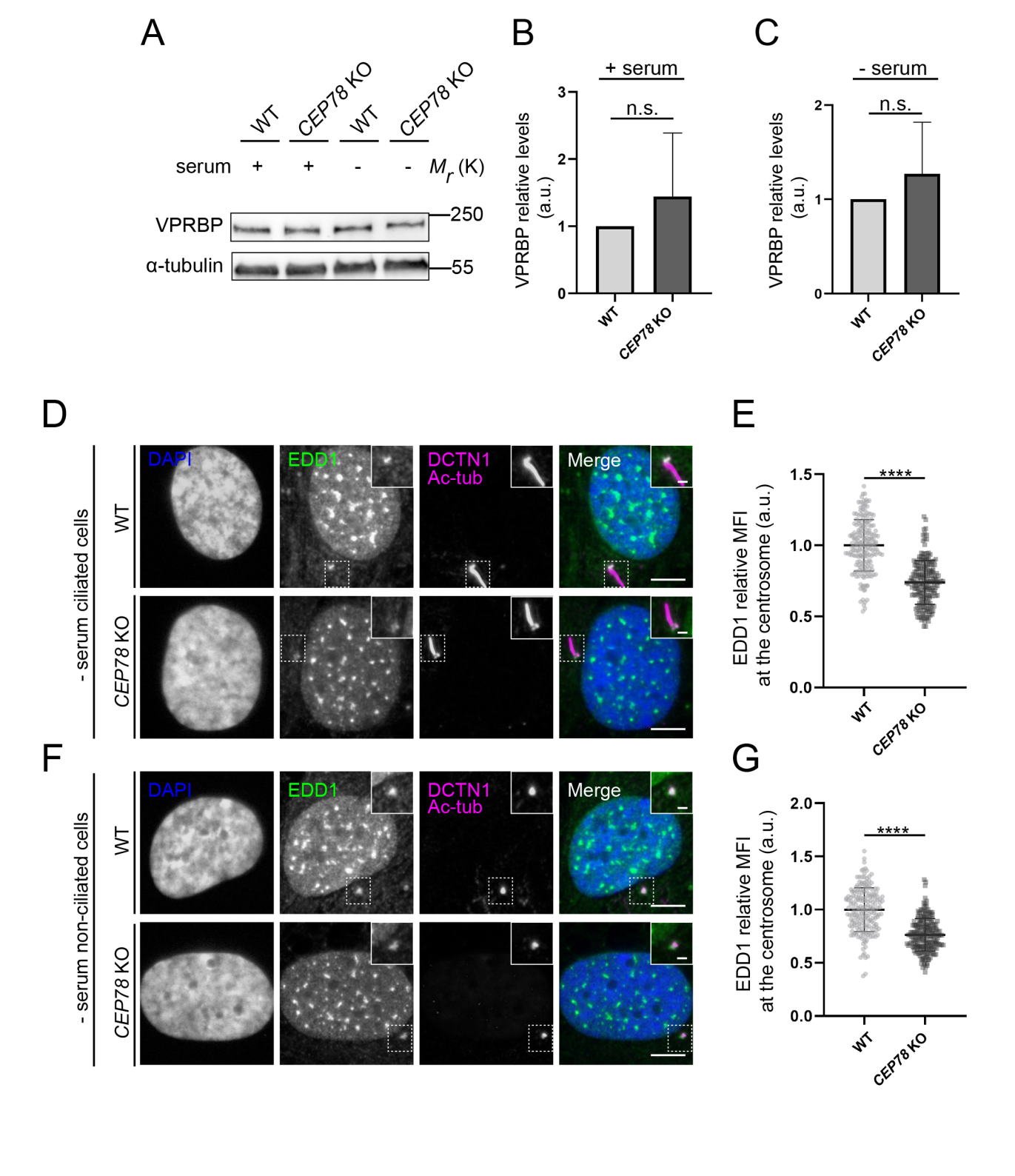
A
WT
CEP78 KO
WT
CEP78 KO
serum
+
+
-
-
M_r (K)
VPRBP
250
α-tubulin
55
B
+ serum
n.s.
VPRBP relative levels (a.u.)
0
1
2
3
WT
CEP78 KO
C
- serum
n.s.
VPRBP relative levels (a.u.)
0
1
2
WT
CEP78 KO
D
- serum ciliated cells
WT
CEP78 KO
DAPI
EDD1
DCTN1
Ac-tub
Merge
E
EDD1 relative MFI at the centrosome (a.u.)
0.0
0.5
1.0
1.5
****
WT
CEP78 KO
F
- serum non-ciliated cells
WT
CEP78 KO
DAPI
EDD1
DCTN1
Ac-tub
Merge
G
EDD1 relative MFI at the centrosome (a.u.)
0.0
0.5
1.0
1.5
2.0
****
WT
CEP78 KO

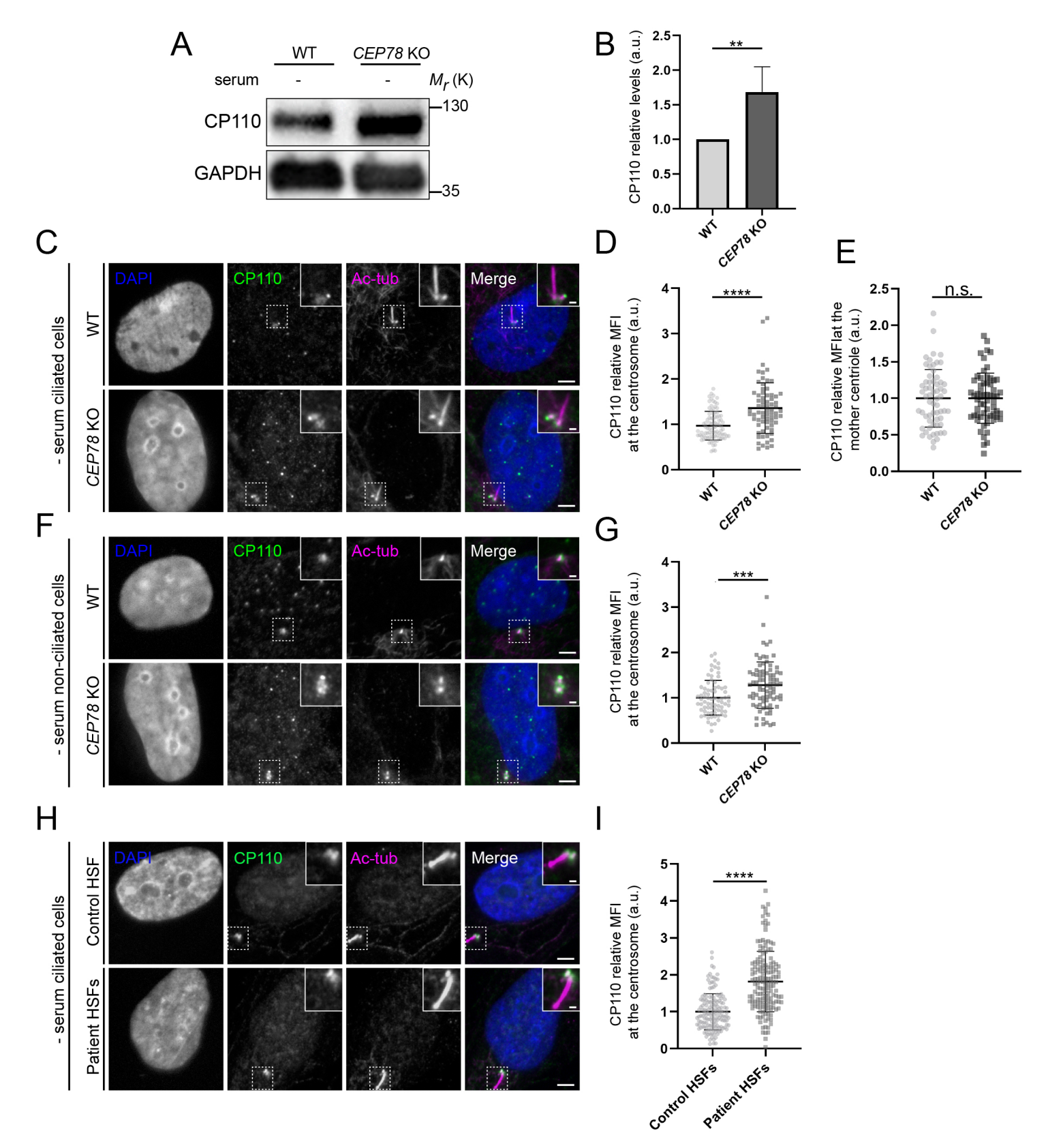
A
WT
CEP78 KO
serum
-
-
Mr (K)
CP110
130
GAPDH
35
B
CP110 relative levels (a.u.)
**
WT
CEP78 KO
C
- serum ciliated cells
WT
CEP78 KO
DAPI
CP110
Ac-tub
Merge
D
CP110 relative MFI at the centrosome (a.u.)
****
WT
CEP78 KO
E
CP110 relative MFIat the mother centriole (a.u.)
n.s.
WT
CEP78 KO
F
- serum non-ciliated cells
WT
CEP78 KO
DAPI
CP110
Ac-tub
Merge
G
CP110 relative MFI at the centrosome (a.u.)
***
WT
CEP78 KO
H
- serum ciliated cells
Control HSF
Patient HSFs
DAPI
CP110
Ac-tub
Merge
I
CP110 relative MFI at the centrosome (a.u.)
****
Control HSFs
Patient HSFs

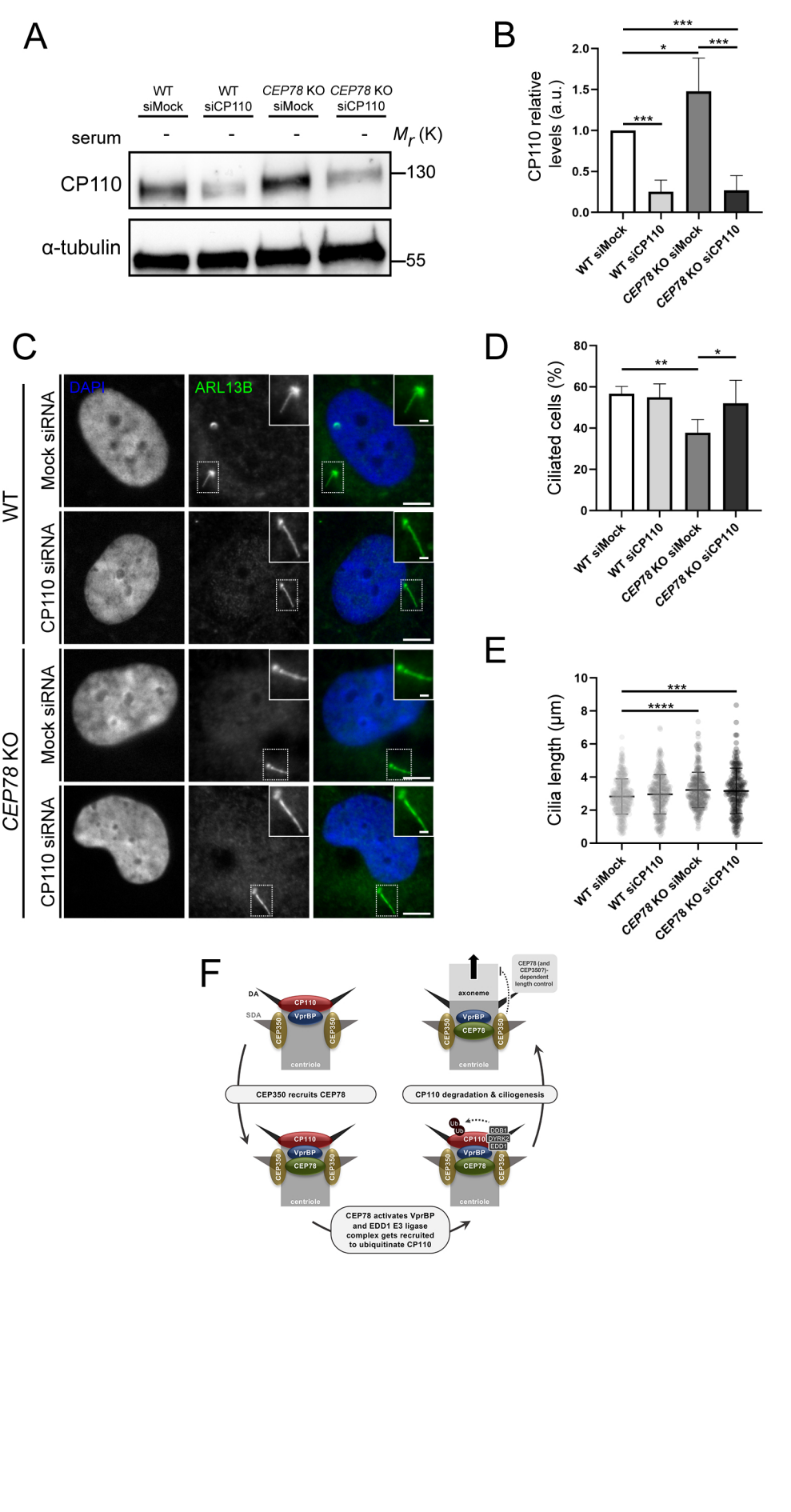
A
WT siMock
WT siCP110
CEP78 KO siMock
CEP78 KO siCP110
serum
-
-
-
-
Mr (K)
CP110
130
α-tubulin
55
B
CP110 relative levels (a.u.)
2.0
1.5
1.0
0.5
0.0
***
*
***
***
WT siMock
WT siCP110
CEP78 KO siMock
CEP78 KO siCP110
C
WT
CEP78 KO
Mock siRNA
CP110 siRNA
Mock siRNA
CP110 siRNA
DAPI
ARL13B
D
Ciliated cells (%)
80
60
40
20
0
**
*
WT siMock
WT siCP110
CEP78 KO siMock
CEP78 KO siCP110
E
Cilia length (μm)
10
8
6
4
2
0
***
****
WT siMock
WT siCP110
CEP78 KO siMock
CEP78 KO siCP110
F
DA
SDA
CP110
VprBP
CEP350
CEP350
centriole
CEP350 recruits CEP78
axoneme
CEP78 (and CEP350?)-dependent length control
CP110 degradation & ciliogenesis
Ub
Ub
DDB1
DYRK2
EDD1
CEP78 activates VprBP and EDD1 E3 ligase complex gets recruited to ubiquitinate CP110